Exhibit A

CHAPTER

14

Glycolysis and the Catabolism of Hexoses

Having examined the organizing principles of cell metabolism and bioenergetics, we are ready to see how the chemical energy stored in glucose and other fuel molecules is released to perform biological work. D-Glucose is the major fuel of most organisms and occupies a central position in metabolism. It is relatively rich in potential energy; its complete oxidation to carbon dioxide and water proceeds with a standard free-energy change of −2,840 kJ/mol. By storing glucose as a high molecular weight polymer, a cell can stockpile large quantities of hexose units while maintaining a relatively low cytosolic osmolarity. When the cell's energy demands suddenly increase, glucose can be released quickly from these intracellular storage polymers.

Glucose is not only an excellent fuel, it is also a remarkably versatile precursor, capable of supplying a huge array of metabolic intermediates, the necessary starting materials for biosynthetic reactions. *E. coli* can obtain from glucose the carbon skeletons for every one of the amino acids, nucleotides, coenzymes, fatty acids, and other metabolic intermediates needed for growth. A study of the numerous metabolic fates of glucose would encompass hundreds or thousands of transformations. In the higher plants and animals glucose has three major fates: it may be stored (as a polysaccharide or as sucrose), oxidized to a three-carbon compound (pyruvate) via glycolysis, or oxidized to pentoses via the pentose phosphate (phosphogluconate) pathway (Fig. 14–1).

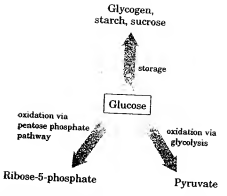

Figure 14–1 Major pathways of glucose utilization in cells of higher plants and animals. Although not the only possible fates for glucose, these three pathways are the most significant in terms of the amount of glucose that flows through them in most cells.

This chapter begins with a description of the individual reactions that constitute the glycolytic pathway and of the enzymes that catalyze them. We then consider fermentation, the operation of the glycolytic pathway under anaerobic conditions. The sources of glucose units for glycolysis are diverse, and we next describe pathways that bring carbon into glycolysis from hexoses other than glucose and from disaccharides and polysaccharides. Like all metabolic pathways, glycolysis is under tight regulation. We discuss the general principles of metabolic regulation, then illustrate these principles with the glycolytic pathway. The chapter concludes with a brief description of two other catabolic pathways that begin with glucose: one leading to pentoses, the other to glucuronate and ascorbic acid (vitamin C).

Glycolysis

In **glycolysis** (from the Greek *glykys*, meaning "sweet," and *lysis*, meaning "splitting") a molecule of glucose is degraded in a series of

enzyme-catalyzed reactions to yield two molecules of pyruvate. During the sequential reactions of glycolysis some of the free energy released from glucose is conserved in the form of ATP. Glycolysis was the first metabolic pathway to be elucidated and is probably the best understood. From the discovery by Eduard Buchner (in 1897) of fermentation in broken extracts of yeast cells until the clear recognition by Fritz Lipmann and Herman Kalckar (in 1941) of the metabolic role of high-energy compounds such as ATP in metabolism, the reactions of glycolysis in extracts of yeast and muscle were central to biochemical research. The development of methods of enzyme purification, the discovery and recognition of the importance of cofactors such as NAD, and the discovery of the pivotal role in metabolism of phosphorylated compounds all came out of studies of glycolysis. By now, all of the enzymes of glycolysis have been purified from many organisms and thoroughly studied, and the three-dimensional structures of all of the glycolytic enzymes are known from x-ray crystallographic studies.

Fritz Lipmann
1899–1986

Herman Kalckar
1908–1991

Glycolysis is an almost universal central pathway of glucose catabolism. It is the pathway through which the largest flux of carbon occurs in most cells. In certain mammalian tissues and cell types (erythrocytes, renal medulla, brain, and sperm, for example), glucose is the sole or major source of metabolic energy through glycolysis. Some plant tissues that are modified for the storage of starch (such as potato tubers) and some plants adapted to growth in areas regularly inundated by water (watercress, for example) derive most of their energy from glycolysis; many types of anaerobic microorganisms are entirely dependent on glycolysis.

Fermentation is a general term denoting the *anaerobic* degradation of glucose or other organic nutrients into various products (characteristic for different organisms) to obtain energy in the form of ATP. Because living organisms first arose in an atmosphere lacking oxygen, anaerobic breakdown of glucose is probably the most ancient biological mechanism for obtaining energy from organic fuel molecules. In the course of evolution this reaction sequence has been completely conserved; the glycolytic enzymes of vertebrate animals are closely similar, in amino acid sequence and three-dimensional structure, to their homologs in yeast and spinach. The process of glycolysis differs from one species to another only in the details of its regulation and in the subsequent metabolic fate of the pyruvate formed. The thermodynamic principles and the types of regulatory mechanisms in glycolysis are found in all pathways of cell metabolism. A study of glycolysis can serve as a model of many aspects of the pathways discussed later in this book.

Before examining each step of the pathway in some detail, we will take a look at glycolysis as a whole.

An Overview: Glycolysis Has Two Phases

The breakdown of the six-carbon glucose into two molecules of the three-carbon pyruvate occurs in ten steps, the first five of which constitute the *preparatory phase* (Fig. 14–2a). In these reactions glucose is first phosphorylated at the hydroxyl group on C-6 (step ①). The D-glucose-6-phosphate thus formed is converted to D-fructose-6-phosphate (step ②), which is again phosphorylated, this time at C-1, to yield D-fructose-1,6-bisphosphate (step ③). For both phosphorylations, ATP is the phosphate donor. As all of the sugar derivatives that occur in the glycolytic pathway are the D isomers, we will omit the D designation except when emphasizing stereochemistry.

Exhibit B

1: J Anim Sci. 1979;49 Suppl 2:26-34.

Links

Requirements for blastocyst development in vitro.

Brinster RL, Troike DE.

Four characteristics of culture medium that are important to embryo development and nutrition of the blastocyst have been discussed. An examination of several of the most commonly used media for embryo culture demonstrates many similarities among them. The milliosmolarities of the media range from the hypoosmotic optimums (256 milliosmols) demonstrated in several in vitro studies to the physiologic range (308 to 315 milliosmols). Media between these extremes generally allow good development. Low oxygen concentrations (5%) in the culture environment allow somewhat better development of early cleavage stages, but recent studies suggest the difference between development in 5 and 20% oxygen to be less than originally thought. The media most commonly employed for early embryo culture contain bicarbonate as the buffer, but maintenance of pH is probably not the most crucial role of the CO2-bicarbonate content of the media. Likewise, since 1965 almost all media used to culture embryos have used pyruvate as the primary energy source. This is particularly important when early stages, before blastocyst development, are cultured. The concentration used generally falls within the optimum range of 2.5 to 5.0 X 10(-4)M first reported. Although glucose is not oxidized well by the early cleavage stages, it is an important energy source for all blastocysts. Furthermore, glucose contributes more than any other carbon source, including amino acids, to protein formation. Much is yet to be learned concerning the nutrition of the blastocyst, but our knowledge has increased immensely during the last 15 years. Hopefully our progress will be at least as rapid in the coming decade.

PMID: 45481 [PubMed - indexed for MEDLINE]

Exhibit C

1: J Urol. 1986 May;135(5):1057-60.

Effects of pyruvate salts, pyruvic acid, and bicarbonate salts in preventing experimental oxalate urolithiasis in rats.

Ogawa Y, **Yamaguchi K**, **Tanaka T**, **Morozumi M**.

Sodium pyruvate, potassium pyruvate, pyruvic acid, sodium bicarbonate and potassium bicarbonate were added to a calcium-oxalate lithogenic diet (a glycolic-acid diet) in order to determine their effects in preventing lithogenicity. Male Wistar-strain rats who had been fed the glycolic-acid diet developed marked urinary calculi within four weeks. Rats in the sodium and potassium pyruvate groups had, however, almost no stones in the urinary system. Rats in the bicarbonate and pyruvic-acid groups showed slightly less effect than those in the pyruvate groups. Urinary oxalate excretion was high in all the groups during the experiment. The urinary oxalate concentration was relatively higher in the sodium-pyruvate group, and significantly higher in the potassium-pyruvate group, than in the glycolic-acid group. Urinary citrate excretion was high both in the pyruvate and bicarbonate groups; the urinary citrate concentration was, however, significantly higher in the pyruvate groups than in the bicarbonate groups at the fourth experimental week. The urinary calcium and magnesium concentrations were irrelevant to the diets administered. Therefore, it can be concluded that pyruvate salts inhibit urinary calculi formation, not by decreasing oxalate synthesis, but by increasing the urinary citrate concentration; bicarbonate salts work in the same manner, but a little less effectively.

PMID: 3007782 [PubMed - indexed for MEDLINE]

Exhibit D

Effects of pyruvate on the metabolism and insulin resistance of obese Zucker rats[1–3]

John L Ivy, Miriam Y Cortez, Resa M Chandler, Heidi K Byrne, and Robert H Miller

ABSTRACT Female obese Zucker rats aged 5 wk were randomly assigned to a control diet or one of two experimental diets. Experimental diets contained 6% of energy as pyruvate in the form of calcium-pyruvate (Ca-pyr) or 6% pyruvylglycine (pyr-gly). Diets were pair-fed according to the experimental group with the lowest food consumption. During the 3 wk of dietary treatment, Ca-pyr– and pyr-gly–fed rats gained significantly less weight, had a lower food-conversion efficiency, and maintained a higher resting oxygen consumption ($mL \cdot min^{-1} \cdot kg^{-0.67}$) than control rats. Ca-pyr and pyr-gly also lowered the respiratory exchange ratio of the rats resulting in a 90% increase in their lipid oxidation and a 50% decrease in their carbohydrate oxidation. Glucose tolerance, assessed by an oral glucose load, was not different among treatments, but the insulin response of the pyr-gly–fed rats was significantly less than that of the control rats despite elevated plasma triglyceride concentrations in the pyr-gly–fed rats (control, 1.43 ± 0.16 vs pyr-gly, 3.76 ± 0.87 mmol/L). These results suggest that pyr-gly, like Ca-pyr, favorably alters the metabolism of obese Zucker rats. In addition, pyr-gly appeared to reduce the insulin resistance that develops spontaneously in obese rats. *Am J Clin Nutr* 1994;59:331–7.

KEY WORDS Oxygen consumption, resting metabolic rate, glucose, glucose tolerance, cholesterol, triglyceride, glycogen, growth, pyruvate

Introduction

Pyruvate when fed to rats, causes significant alterations in body composition and metabolism. In general, pyruvate increases resting metabolic rate and decreases the rate of growth and percent body fat (1). Recently, we reported that dietary pyruvate caused a significant increase in the resting energy expenditure and a decrease in food-conversion efficiency and rate of weight gain in obese Zucker rats (2). These results suggest that pyruvate treatment has potential as an antiobesity agent. An undesirable aspect of pyruvate, however, is its elevated mineral load when administered as a sodium or calcium salt. In providing a sufficient amount of these pyruvate salts, an inappropriate amount of sodium or calcium is consumed. Possible alternatives to the pyruvate salts are pyruvate analogs that stabilize the pyruvic moeity without accompanying minerals. One such analog is pyruvylglycine with a hydrolyzable amide linkage between pyruvic acid and the amino acid glycine (3, 4). Therefore, the purpose of this study was to determine the effect of pyruvylglycine on the growth rate, resting metabolic rate, and food-conversion efficiency of obese Zucker rats.

In addition to their obesity, Zucker rats are highly insulin resistant, which is manifested by severe hyperinsulinemia, glucose intolerance, and an elevated plasma insulin response to a glucose challenge (5–8). In our previous study we observed that pyruvate consumption reduced the fasting plasma insulin concentration of obese Zucker rats without affecting their normal fasting plasma glucose concentration (2). This finding is in agreement with Stanko and Adibi (1) who found that pyruvate reduced the fasting plasma insulin concentration of non-insulin-resistant male Sprague-Dawley rats by ≈50%. Therefore, a second purpose of this study was to determine if pyruvate or pyruvylglycine consumption would improve the glucose tolerance and the postglucose insulin response of obese Zucker rats.

Methods

Housing and care of animals

Female obese Zucker rats (fa/fa), aged 28–35 d were purchased from Charles River Inc (Boston). Upon arrival the rats were housed in individual cages and provided normal rat food (Ralston Purina Rodent Chow, St Louis) and water ad libitum for 1 wk. An artificial 12-h light-dark cycle was maintained in the animal room and the temperature was kept at 21 °C. After 1 wk of familiarization with their environment, the rats were fed powdered rodent chow. Familiarization with the powdered diet was determined by consistent weight gain for a minimum of 7 d, after which the rats were assigned to one of three dietary treatments. This study was approved by the Animal Care and Use Committee of the University of Texas.

Dietary treatments

The diets were powdered and consisted of a control diet and two experimental diets (**Table 1**). The control diet was composed of 21.7% protein, 12.1% fat, and 66.2% carbohydrate (59% su-

[1] From the Exercise Physiology and Metabolism Laboratory, Department of Kinesiology, The University of Texas at Austin, and Medical Nutrition Research and Development, Ross Laboratories, Columbus, OH.

[2] Supported by a grant from Ross Laboratories, Columbus, OH.

[3] Address reprint requests to JL Ivy, Department of Kinesiology, Bellmont Hall 222, The University of Texas at Austin, Austin, TX 78712.

Received September 10, 1992.
Accepted for publication July 22, 1993.

TABLE 1
Composition of control and experimental diets*

Diet composition	Control	Ca-pyr	Pyr-gly
		g/kg	
Alcohol-extracted casein	200	200	200
DL-methionine	3	3	3
Corn starch	250	250	250
Cellulose	50	50	50
Corn oil	50	50	50
Vitamin mix	10	10	10
Choline bitartrate	2	2	2
Salt mix	5	5	5
Sucrose	358	310	236
Calcium phosphate	72	30	72
Calcium pyruvate	0	90	0
Pyruvylglycine	0	0	122

* Ca-pyr, calcium pyruvate diet; pyr-gly, pyruvylglycine diet. The control diet provided 15.61 kJ/g, the Ca-pyr diet 15.78 kJ/g, and the pyr-gly diet 15.57 kJ/g.

crose and 41% starch), and was fortified with vitamin and mineral mixes (Research Diets, Inc, New Brunswick, NJ). In the two experimental diets calcium-pyruvate (Ca-pyr) or pyruvylglycine (pyr-gly) was substituted for sucrose so that pyruvate represented 6% of the total energy. Rats were pair-fed to match the pyr-gly group because this group had the lowest voluntary food consumption during the first 3 d of treatment. Food bowls were replenished with the diets daily between 0800 and 1000. Food consumption for the previous day and body weights of the rates were recorded at this time. The rats were maintained on the diets for 3 wk.

Metabolic measurements

Before the rats were placed on their experimental diets and again 4 d before the conclusion of their treatment period, resting oxygen consumption ($\dot{V}O_2$) and respiratory exchange ratio (R) were determined by open-circuit spirometry after a 5-h fast. To ensure an accurate measure of resting energy expenditure, the rats were tested 3–4 h into their light cycle. Five rats were placed into five separate metabolic chambers. A description of the metabolic chamber was published previously (2). During the measurement of $\dot{V}O_2$, air flow through the chamber was maintained at 0.85 L/min by an air sampling pump (Dwyer Instruments Inc, Michigan City, IN). The pump was calibrated with an airflow meter (Vacumetrics, Ventura, CA), which in turn was calibrated with a chain-compensated spirometer (Warren E Collins, Braintree, MA). Tubing from the outlet port of the pump was connected to a Y tube. Approximately 0.15 L/min air was directed through an air-tight three-way valve attached to a CD-3A carbon dioxide analyzer and a S-3A/1 oxygen analyzer (Applied Electrochemistry-Amtex, Pittsburgh). The remaining 0.70 L was expelled as exhaust. Gas values were read from each of the five chambers in a sequential manner during the final 15 s of a 2-min sample period. A total of five to six measurements were taken for each rat over a 2-h period. The gas analyzers were frequently checked for calibration throughout the measurement period by using gases verified by chemical analysis. $\dot{V}O_2$ and carbon dioxide production ($\dot{V}CO_2$) were calculated according to Brooks and White (9). R was calculated as $\dot{V}CO_2/\dot{V}O_2$. Chamber temperature was monitored with a flexible thermister (Yellow Springs Instruments, Yellow Springs, OH) inserted into a recessed opening in the front wall of the chamber.

To allow for adequate ventilation of the chambers between $\dot{V}O_2$ measurements, a vacuum pump (Universal Electric Co, Owosso, MI) drew air through the four additional metabolic chambers, which were connected in parallel, at 0.75 L/min per chamber. All of the air drawn through the pump was expelled as exhaust from the outlet port.

Tissue collection

Before the dietary treatments and after an 8-h fast, the tails of the rats were trimmed and 0.7 mL blood was collected in tubes containing 40 μL EDTA (pH 7.4, 24 g/L). The blood was kept on ice until centrifuged at 1000 × g (4 °C) for 12 min. The plasma was recovered and stored at −80 °C until assayed for glucose, insulin, cholesterol, and triglycerides.

After 3 wk of dietary treatments, and after an 8-h fast, the rats underwent an oral glucose-tolerance test (OGTT). The rats were intubated with 1 g glucose/kg body wt from a 50% glucose solution. Tail blood samples (0.7 mL) were collected in tubes containing 40 μL EDTA before intubation and at 15, 30, and 60 min after glucose intubation. The blood was kept on ice until centrifuged as described above and later assayed for insulin and glucose. Blood samples taken before the intubation were also assayed for triglycerides and cholesterol. After the OGTT, 1.5 mL of saline solution was injected subcutaneously behind the neck of each rat to prevent dehydration and help maintain plasma volume.

Two days after the OGTT, and after an 8-h fast, the rats were anesthetized with an intraperitoneal injection of 0.65 g pentobarbital sodium/g body wt (Fort Dodge Laboratories, Inc, Fort Dodge, IA). From the left hindlimb, the popliteal fat depot (a peripheral fat depot), soleus, plantaris, and gastrocnemius were removed. The popliteal fat pad was weighed and discarded. The soleus and plantaris muscles were freeze-clamped with tongs cooled in liquid nitrogen and stored at −80 °C for subsequent determination of glycogen. Red and white portions of the gastrocnemius were dissected, freeze-clamped, and stored as described above for determination of glycogen. The remainder of the gastrocnemius was weighed and discarded. Next, the abdomen was surgically opened and a portion of the left lateral lobe of the liver was excised, freeze-clamped, and stored at −80 °C. The remainder of the liver was then excised, weighed, and discarded. The frozen liver section was assayed for glycogen, triglycerides, and cholesterol. Finally, the left retroperitoneal fat pad (an internal fat pad) was removed, weighed, and discarded.

Tissue analysis

Plasma glucose was measured with a model 23A glucose analyzer (Yellow Springs Instruments). Plasma insulin was determined by radioimmunoassay with the use of a double-antibody procedure (10) (antibodies were obtained from Linco Research, Inc, St Louis). Rat insulin was used as a standard. Plasma triglycerides and cholesterol concentrations were enzymatically determined with the use of commercially available kits (Sigma Diagnostics, St Louis).

Liver homogenates were prepared in buffer containing 50 mmol/potassium phosphate/L and 1 mmol EDTA/L (pH 7.4, 1:15). The lipid was extracted from the homogenate according

to the procedures of Burton et al (11). The lipid extract was evaporated at room temperature for 24 h and resuspended in 2-propanol. Liver triglyceride content was determined from the resuspended extracts as described above for plasma. Liver and muscle glycogen were determined by the method of Lo et al (12).

Statistics

For statistical analysis, a one- or two-way analysis of variance with repeated measures was used where appropriate. Fisher's protected least-significant difference (PLSD) test was subsequently used to locate significant differences between means. A P level < 0.05 was set for significance for all tests, and all values are expressed as mean ± SEM. The *Stat View 512*+ computer software program (Calabasas, CA) was used for all analyses.

Results

Despite the pair-feeding regimen, during the 3-wk experimental treatment period, the average weight gains of the Ca-pyr and pyr-gly rats were significantly less than those of the control rats (Table 2). The differences, however, were mainly due to a weight loss during the first 4–5 d of feeding the experimental diets (Fig 1). During this period there was a decline in the body weights of the pyr-fed rats, whereas the control rats continued to gain weight. After this initial decline in body weight, the pyr-fed rats started to gain weight but at a slower rate than that of the control rats. This difference in weight gain between the pyr-fed and control rats persisted for the next 12 d (control, 42.3 ± 2.1; Ca-pyr, 33.1 ± 4.3; pyr-gly, 32.2 ± 3.3 g/12 d). Thereafter, the rate of weight gain for the pyr-fed and control rats were similar due to a reduction in the rate of weight gain of the control rats.

The soleus and gastrocnemius muscles of the Ca-pyr and pyr-gly rats were significantly smaller than those of the control rats (Table 2). The popliteal fat depots of the Ca-pyr and pyr-gly rats and the retroperitoneal fat pad of the pyr-gly rats were also smaller than those of the control rats. The livers of the Ca-pyr rats, but not those of the pyr-gly rats, were smaller than the livers

TABLE 2
Body, organ, and muscle weights of diet groups*

	Control (n = 8)	Ca-pyr (n = 7)	Pyr-gly (n = 8)
Body weight (g)			
Initial	251.8 ± 10.3	246.1 ± 9.2	245.3 ± 9.1
Final	324.3 ± 11.9	290 ± 7.1†	285.9 ± 10.2†
Soleus			
(g)	0.091 ± 0.005	0.075 ± 0.002†	0.076 ± 0.003†
(% body wt)	0.028 ± 0.002	0.027 ± 0.002	0.027 ± 0.001
Gastrocnemius			
(g)	0.628 ± 0.032	0.515 ± 0.025†	0.516 ± 0.010†
(% body wt)	0.194 ± 0.009	0.178 ± 0.006	0.183 ± 0.007
Liver			
(g)	17.57 ± 1.00	15.16 ± 0.77†	17.62 ± 0.74
(% body wt)	5.43 ± 0.27	5.22 ± 0.22	6.18 ± 0.24†
Retroperitoneal fat pad			
(g)	3.10 ± 0.13	2.73 ± 0.11	2.51 ± 0.23†
(% body wt)	0.96 ± 0.04	0.95 ± 0.05	0.87 ± 0.06
Popliteal fat depot			
(g)	1.17 ± 0.12	0.94 ± 0.04†	0.93 ± 0.06†
(% body wt)	0.36 ± 0.03	0.32 ± 0.01	0.32 ± 0.01

* $\bar{x}$ ± SEM. Ca-pyr, calcium pyruvate; pyr-gly, pyruvylglycine.
† Significantly different from control group, $P < 0.05$.

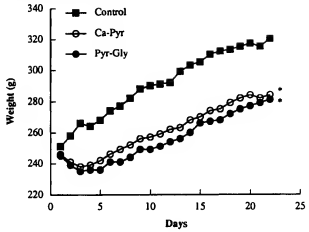

FIG 1. Body weights of the three dietary groups from days 1 to 22. Control diet; Ca-pyr, calcium pyruvate diet; pyr-gly, pyruvylglycine diet. *Significantly different from control, $P < 0.05$.

of the control rats. When made relative to body weight, there were no differences between the muscle or fat pad weights of the Ca-pyr, pyr-gly, or control rats. The relative liver weights of the pyr-gly rats, however, were larger than those of the control rats.

The average daily food consumption was significantly reduced by the addition of the experimental compounds to the diets. Although an effort was made to pair-feed the rats, the experimental groups (17.3 ± 0.62 g/d, Ca-pyr; 16.9 ± 0.41 g/d, pyr-gly) consumed less food than the control rats (18.5 ± 0.27 g/d) (control vs pyr-gly, $P < 0.05$). Food consumption was not different between the Ca-pyr or pyr-gly rats. The reason for the difference in food consumption was due to the first few days of feeding when the control rats were consuming 22–24 g food and the pyr-fed rats were consuming only 7–10 g. After this initial period, food consumption did not differ between groups.

Pretreatment resting VO_2 was not different among treatments (Table 3) whether expressed as absolute (mL/min) or relative to metabolic weight ($mL \cdot min^{-1} \cdot kg^{-0.67}$). After the 3-wk experimental period, the absolute resting VO_2 did not change, but VO_2 significantly declined in all groups when made relative to the size of the rat. The decline was greater for the control rats (23%) than for the experimental groups (Ca-pyr 14%, pyr-gly 16%). This decline resulted in the post-VO_2 and resting energy expenditure of the pyr-gly rats being significantly higher compared with the control rats. Although the difference in relative VO_2 between the Ca-pyr and control rats posttreatment was not significant, it approached significance ($P < 0.08$). There was no difference in resting energy expenditure between the Ca-pyr and pyr-gly rats. Both the Ca-pyr and pyr-gly rats had lower food-conversion efficiencies (wt gain/wt food consumed × 100) than the control rats (Fig 2).

R was not different among groups before the start of the experimental treatments, but by the third week of treatment rats in the experimental groups demonstrated significantly lower resting R values compared with control rats (Table 3). Calculations of substrate utilization based on R and VO_2 indicated that the rats in the experimental groups oxidized significantly less carbohydrate and significantly more fat than control rats. No differences were noted between the Ca-pyr and pyr-gly rats.

TABLE 3
Resting oxygen consumption ($\dot{V}O_2$), energy expenditure, and substrate utilization estimated from the nonprotein respiratory-exchange ratio (R) before and after dietary treatments in obese Zucker rats*

	Control (n = 8)	Ca-pyr (n = 7)	Pyr-gly (n = 8)
$\dot{V}O_2$			
Before (mL/min)	3.40 ± 0.27	3.48 ± 0.16	3.73 ± 0.10
After (mL/min)	3.30 ± 0.25	3.45 ± 0.13	3.28 ± 0.12
Before (mL·min^{-1}·kg$^{-0.67}$)	9.12 ± 0.63	9.31 ± 0.32	9.77 ± 0.32
After (mL·min^{-1}·kg$^{-0.67}$)	7.05 ± 0.44	8.00 ± 0.25	8.20 ± 0.19†
R			
Before	0.846 ± 0.027	0.838 ± 0.021	0.855 ± 0.015
After	0.859 ± 0.025	0.771 ± 0.009†	0.777 ± 0.009†
Energy expenditure after (J·min^{-1}·kg^{-1})	209.3 ± 12.5	242.8 ± 8.4†	247.0 ± 12.5†
Carbohydrate after (mg·min^{-1}·kg^{-1})	6.41 ± 1.15	3.09 ± 0.44†	3.47 ± 0.57†
Fat after (mg·min^{-1}·kg^{-1})	2.51 ± 0.49	4.79 ± 0.23†	4.69 ± 0.30†

* $\bar{x}$ ± SEM. Ca-pyr, calcium pyruvate; pyr-gly, pyruvylglycine.
† Significantly different from control group, $P < 0.05$.

No differences in pretreatment plasma triglyceride or cholesterol concentrations were found among groups (**Table 4**). Post-treatment plasma triglyceride concentrations declined whereas plasma cholesterol concentrations increased. No differences were noted between treatments for plasma cholesterol, but the plasma triglyceride concentrations of the pyr-gly rats declined to a significantly lesser extent than those of the Ca-pyr and control rats.

There were no differences in the plasma insulin and glucose concentrations between groups before the experimental treatments with the exception that pyr-gly rats had a higher plasma glucose concentration than control rats (Table 4). After the 3 wk of dietary treatment and before the OGTT, plasma insulin concentrations for the Ca-pyr and pyr-gly rats were significantly lower than those of the control rats despite no differences in plasma glucose concentrations (Table 4; **Fig 3**). During the OGTT, plasma glucose responses were similar for all treatments (Fig 3). However, the insulin response for the Ca-pyr and pyr-gly rats was significantly lower than that of the control rats at 30 min post-glucose intubation. The insulin response of the pyr-gly rats was also lower than that of the control rats at 60 min postintubation. There were no differences in the areas under the glucose response curves for the three treatments (**Table 5**). The total area under the insulin response curve of the pyr-gly rats, however, was significantly lower than the area under the insulin response curve of the control rats. Furthermore, the insulin-glucose (IG) index of the pyr-gly rats was significantly lower than that of the control rats.

Rats fed the experimental diets had liver triglyceride and cholesterol concentrations similar to those of control rats when expressed as μmol/g wet wt or in total mmol (**Table 6**). Liver glycogen concentrations, however, were significantly lower in the pyr-gly rats as compared with the control rats whether expressed as μmol/g wet wt or in total mmol. The liver glycogen concentration of the Ca-pyr rats did not differ from either the control or the pyr-gly rats.

Muscle glycogen concentrations were determined for the soleus and the red and white portions of the gastrocnemius (**Table 7**). No differences were noted among the three treatments with the exception that the red gastrocnemius glycogen concentration

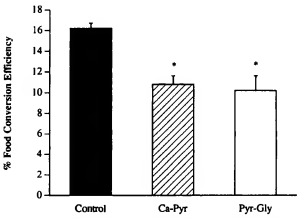

FIG 2. Average food-conversion efficiency (weight gain per food consumed × 100) for the three dietary groups during the 3 wk of experimental treatment. Control diet; Ca-pyr, calcium pyruvate diet, pyr-gly, pyruvylglycine diet. *Significantly different from control, $P < 0.05$.

TABLE 4
Plasma lipids, insulin, and glucose concentrations before and after dietary treatments in obese Zucker rats

	Control (n = 8)	Ca-pyr (n = 7)	Pyr-gly (n = 8)
Insulin (nmol/L)			
Before	1.14 ± 0.12	1.09 ± 0.13	0.94 ± 0.07
After	1.89 ± 0.15	1.40 ± 0.09†	1.12 ± 0.13†
Glucose (mmol/L)			
Before	6.5 ± 0.2	7.3 ± 0.3	7.4 ± 0.3†
After	6.4 ± 0.6	6.6 ± 0.5	6.2 ± 1.1
Triglycerides (mmol/L)			
Before	7.23 ± 1.25	7.35 ± 1.59	5.56 ± 0.80
After	1.43 ± 0.16	1.49 ± 0.16	3.76 ± 0.87†‡
Cholesterol (mmol/L)			
Before	4.32 ± 0.15	3.89 ± 0.31	4.23 ± 0.35
After	8.65 ± 0.74	7.94 ± 0.47	7.69 ± 0.36

* $\bar{x}$ ± SEM. Ca-pyr, calcium pyruvate and pyr-gly, pyruvylglycine.
† Significantly different from control; ‡significantly different from Ca-pyr, $P < 0.05$.

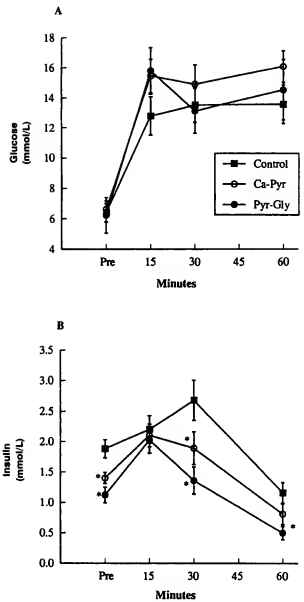

FIG 3. Plasma glucose (A) and insulin (B) responses of the three dietary groups to an oral glucose-tolerance test. Control diet; Ca-pyr, calcium pyruvate diet; pyr-gly, pyruvylglycine diet. *Significantly different from control, $P < 0.05$.

of the Ca-pyr rats was greater than that of the control rats. It was also noted that the white gastrocnemii glycogen concentrations were greater than those of the red gastrocnemii, which were greater than those of the solei.

Discussion

A major finding of this study was that pyr-gly was as effective, and in some instances more effective, than Ca-pyr in altering the growth pattern and metabolic activity of obese Zucker rats. Both Ca-pyr and pyr-gly caused a significant decline in the average weight gain of the obese Zucker rats during the 22 d of treatment.

TABLE 5
Total areas for plasma glucose and insulin responses during an oral glucose-tolerance test in obese Zucker rats*

	Control (n = 8)	Ca-pyr (n = 7)	Pyr-gly (n = 8)
Total glucose area (mmol · L^{-1} · min^{-1})	748 ± 58	858 ± 54	790 ± 88
Total insulin area (nmol · L^{-1} · min^{-1})	125 ± 12	96 ± 8	79 ± 7†
Insulin-glucose index (×10^{-3})	94.2 ± 10.9	83.3 ± 9.4	59.6 ± 4.4†

* $\bar{x}$ ± SEM. Ca-pyr, calcium pyruvate and pyr-gly, pyruvalglycine. Glucose-insulin index is the product of the glucose and insulin areas.
† Significantly different from control, $P < 0.05$.

The major difference in weight gain between the pyr-fed rats, whether the mineral salt or analog, and those fed the control diet occurred during the first 4–5 d of treatment. During this period the pyr-fed rats had a decline in body weight whereas the control rats had an increase in body weight. Food consumption was two- to threefold greater for the control rats compared with the pyr-fed rats during the first 3 d when all rats were fed ad libitum. Thereafter, all rats were pair-fed according to the food consumption of the pyr-gly rats. After what appeared to be an adaptation to the experimental diets, the energy consumption and growth rates of the pyr-fed rats increased. However, their growth rates were still less than those of the control rats for the next 11–12 d despite similar energy consumption. Over the last 6 d of the experimental period, the growth rates of the control and pyr-fed rats did not differ due to a decline in the growth rate of the control rats.

As previously noted, the reduced rate of weight gain in the pyr-fed rats appeared to be the result of an overall decrease in growth development with little change in relative body composition (2). This is evinced by the finding that the ratios of individual muscle weights and fat pad weights to body weight were not different for the three dietary groups. It is possible, however, that simple muscle and fat pad weights may not be representative of changes in body composition. Therefore, further study is nec-

TABLE 6
Liver triglyceride, cholesterol, and glycogen concentrations of obese Zucker rats*

	Control (n = 8)	Ca-pyr (n = 7)	Pyr-gly (n = 8)
Triglyceride (μmol/g wet wt)	104.8 ± 5.9	115.3 ± 9.3	111.4 ± 6.1
Trigtyceride (mmol)	1.85 ± 0.17	1.76 ± 0.17	1.98 ± 0.16
Cholesterol (μmol/g wet wt)	9.01 ± 0.49	8.78 ± 0.57	8.57 ± 0.56
Cholesterol (mmol)	0.160 ± 0.015	0.134 ± 0.013	0.102 ± 0.013
Glycogen (μmol/g wet wt)	176.64 ± 21.84	144.47 ± 29.77	110.47 ± 6.84†
Glycogen (mmol)	3.03 ± 0.35	2.31 ± 0.52	1.94 ± 0.14†

* $\bar{x}$ ± SEM. Ca-pyr, calcium pyruvate and pyr-gly, pyruvylglycine.
† Significantly different from control, $P < 0.05$.

TABLE 7
Muscle glycogen concentrations of obese Zucker rats*

	Control (n = 8)	Ca-pyr (n = 7)	Pyr-gly (n = 8)
Soleus (μmol/g wet wt)	25.14 ± 1.27	27.49 ± 2.72	26.73 ± 1.66
Gastrocnemius (μmol/g wet wt)			
Red	32.96 ± 1.08	38.35 ± 2.72†	35.40 ± 0.91
White	43.12 ± 3.40	46.99 ± 2.65	42.41 ± 1.70

* $\bar{x}$ ± SEM. Ca-pyr, calcium pyruvate and pyr-gly, pyruvylglycine.
† Significantly different from control, $P < 0.05$.

essary to determine whether pyruvate feedings can alter the total fat-body weight ratio as well as reduce overall growth rate.

As with our previous study, the food-conversion efficiency of the pyr-fed rats was significantly less than that of the control rats (2). That is, the weight gain per energy consumption was lower in the experimental rats as compared with the control rats. This difference in food-conversion efficiency appeared to be due to a difference in resting energy expenditure. Absolute resting $\dot{V}O_2$ was unchanged during the 3 wk of treatment, but relative resting $\dot{V}O_2$ declined significantly in both the pyr-fed and control rats. The decline, however, was greater in the control rats than in the pyr-fed rats even when the resting $\dot{V}O_2$ was corrected for metabolic body size ($kg^{0.67}$) (13). This resulted in a higher resting $\dot{V}O_2$ for the pyr-fed rats as compared with the control rats by the end of the experimental period.

A depression in resting metabolic rate is a commonly found adaptation after food restriction (14, 15). Typically, the degree to which the resting metabolic rate is reduced is directly related to the degree of food restriction and reduction in weight gain (14). The greater the food restriction and reduction in weight gain, the greater the decline in resting metabolic rate. However, in the present study this relationship was impeded by dietary pyruvate. Although the pyr-fed rats had a slower weight gain and a slightly smaller food consumption than the control rats, their resting $\dot{V}O_2$, even when corrected for body mass, was greater than that of the control rats. These results suggest that dietary pyruvate is a strong activator of metabolism and therefore may be beneficial for weight-reduction programs. However, there may be unknown side effects of long-term use of pyruvate or one of its analogs that are not evident at this time.

It should be noted that the resting metabolic rate of obese rats in the present study was ≈30% less than that previously reported from our laboratory (2). This difference may have been due to the different times within the light-dark cycle that testing was performed. In the present study the rats were tested 3–4 h into their light cycle, when generally very sedentary. In our previous study the rats were tested at the end of their dark cycle and at the beginning of their light cycle, a more active period of time for the rats. Differences in the initial sizes of the rats, the hours of fasting before testing and the basic compositions of the diets may also have contributed to the differences.

Aside from suppressing the decline in metabolic rate of obese Zucker rats, pyruvate significantly reduced the resting R. No significant change in R was noted for the control rats, indicating that the reduction in R in the pyr-fed rats was not due to food restriction. The lower R indicated a 90% increase in lipid oxidation and a 50% decrease in carbohydrate oxidation in the pyr fed rats as compared with the control rats. This increased reliance on fat and reduced reliance on carbohydrate during resting metabolism may have been related to the lower plasma insulin and liver glycogen concentrations observed for the pyr-fed rats. Insulin increases glucose clearance and oxidation by peripheral tissues and inhibits lipolysis (16). Therefore, a lower plasma insulin concentration should shift metabolism in favor of lipid oxidation. The lower liver glycogen concentration should also favor this shift. A reduced liver glycogen concentration should reduce the rate of glucose release from the liver, thus requiring less glucose to be cleared and oxidized by the peripheral tissues to maintain a normal blood glucose concentration. Pyruvate has also been found to increase the rate of muscle glycogen storage which could effectively reduce the rate of carbohydrate oxidation by shifting intracellular glucose disposal from glucose oxidation to storage (17). However, this last possibility is unlikely because the amount of muscle glycogen was not different between treatments.

No differences in the plasma and liver triglycerides and cholesterol concentrations were observed among the treatment groups with the exception that the plasma triglyceride concentrations of the pyr-gly rats were significantly greater than those of the control and Ca-pyr rats after the 3 wk of treatment. The reason for this difference in response is unknown, but could be due to a greater mobilization or reduced clearance of lipid by the pyr-gly rats. It was also found that plasma triglycerides fell and plasma cholesterol rose during the 3 wk of treatment. The decline in plasma triglycerides was probably caused by the decline in food consumption by the obese rats or the use of purified diets. This reduced food consumption may have also resulted in the rise in plasma cholesterol. Previous results from our laboratory have indicated that food-restricted obese rats have lower plasma triglyceride and higher plasma cholesterol concentrations than those fed ad libitum (2). However, Rogers and Kris-Etherton (18) found that 6 wk of food restriction, severe enough to result in a significant loss in body weight, had no effect on the plasma cholesterol concentration of obese Zucker rats. These results suggest that the type of diet the rats receive may also influence the effect of food restriction on plasma cholesterol.

An important finding of this study was the possible increase in insulin action associated with the dietary pyruvate. This increased insulin action was particularly evident in the pyr-gly rats. Both Ca-pyr and pyr-gly rats had lower resting plasma insulin concentrations than control rats despite no increase in plasma glucose concentrations. In fact, the plasma glucose concentration of the pyr-gly rats fell significantly during the 3 wk of dietary treatment. Although no differences in glucose tolerance were found among treatments, the pyr-gly rats had a significantly lower insulin response than the control rats and a significantly lower IG index. The insulin response and IG index of the Ca-pyr rats were intermediate to and not significantly different from that of the control and pyr-gly rats.

The postabsorptive plasma insulin concentration is a function of the rate of endogenous glucose production and the effectiveness of insulin to control its release from the liver (19). Therefore, the reduced postabsorption insulin concentration in the pyr-fed rats may have been a consequence of the reduced liver glycogen stores. An increased muscle glucose extraction at rest and during exercise has been reported for individuals who consumed a pyruvate-dihydroxyacetone supplement for 7 d (17, 20). Because muscle is primarily responsible for the clearance of an oral glucose load (21), it is possible that the reduced insulin response of

the pyr-gly rats to the glucose challenge was due to a reduction in the muscle insulin resistance of obese Zucker rats.

Another possibility for the decreased insulin response of the pyr-gly rats is that there was a faster rate of insulin removal rather than a slower rate of insulin secretion. The liver is the major site of insulin clearance, and it was found that the livers of the pyr-gly rats were ≈15% larger than the livers of the control and Ca-pyr rats when body weight was adjusted for. Therefore, the lower insulin concentrations post-glucose challenge for the pyr-gly rats could have been due to an increased insulin clearance as a result of the increased liver mass. Direct assessment of the effects of pyruvate feeding on muscle insulin resistance is needed to properly address this question.

Although the effect of pyr-gly on the insulin resistance of obese Zucker rats is encouraging, it must be viewed with caution. The addition of pyr-gly to the diet was counterbalanced with the removal of sucrose. Diets composed of high amounts of sucrose have been found to result in impaired in vivo insulin action, hyperinsulinemia, and liver and muscle insulin resistance when compared with diets comprised predominately of starch (22–25). In the present study sucrose comprised 38% and 26% of the total energy of the control and pyr-gly diets, respectively. Whether this small reduction in dietary sucrose could have aided in the improvement in insulin resistance of the pyr-gly rats is unknown but must be considered.

In summary, pyr-gly was found to be as effective as Ca-pyr in reducing the food-conversion efficiency, slowing the weight gain, and maintaining the resting metabolic rate of obese Zucker rats. An unexpected consequence of the pyr-gly treatment was an elevation in the plasma triglyceride concentration. However, despite elevating the plasma triglyceride concentration, pyr-gly appeared to significantly lower the insulin resistance of obese Zucker rats as evinced by the reduced postabsorptive plasma insulin concentration and the insulin response to an oral glucose load. Therefore, the pyruvate analog, pyruvylglycine, may be an important supplement in the treatment of insulin resistance and associated obesity.

We thank Eric Schroeder for his excellent technical assistance.

References

1. Stanko RT, Adibi SA. Inhibition of lipid accumulation and enhancement of energy expenditure by the addition of pyruvate and dihydroxyacetone to a rat diet. Metabolism 1986;35:182–6.
2. Cortez MY, Torgan CE, Brozinick JT Jr, Miller RH, Ivy JL. Effects of pyruvate and dihydroxyacetone consumption on the growth and metabolic state of obese Zucker rats. Am J Clin Nutr 1991;53:847–53.
3. Bergmann M, Grafe K. The connection of racemic acid with amino acid. (Verbindungen von Brenztraubensäure mit Aminosäuren.) Z Physiol Chem 1930;187:196–202.
4. Dixon HBF. Transamination of peptides. Biochem J 1964;92:661–6.
5. Zucker LM, Antoniades HN. Insulin and obesity in the Zucker genetically obese rat "Fatty". Endocrinology 1972;90:1320–9.
6. Ionescu E, Sauter JF, Jeanrenaud B. Abnormal oral glucose tolerance in genetically obese (fa/fa) rats. Am J Physiol 1985;248:E500–6.
7. Becker-Zimmermann K, Berger M, Berchtold P, Gries FA, Herberg L, Schwenen M. Treadmill training improves intravenous glucose tolerance and insulin sensitivity in fatty Zucker rats. Diabetologia 1982;22:468–74.
8. Cortez MY, Torgan CE, Brozinick JT Jr, Ivy JL. Insulin resistance of obese Zucker rats exercise trained at two different intensities. Am J Physiol 1991;261:E613–9.
9. Brooks GA, White TP. Determination of metabolic and heart rate responses of rats to treadmill exercise. J Appl Physiol 1970;45:1009–15.
10. Morgan CR, Lazarow A. Immunoassay of insulin: two antibody system: plasma insulin levels in normal, subdiabetic and diabetic rats. Diabetes 1963;12:115–26.
11. Burton GW, Webb A, Ingold KU. Methods: a mild, rapid and efficient method of lipid extraction for use in determining vitamin E/lipid ratios. Lipid 1985;20:29–39.
12. Lo S, Russell JC, Taylor AW. Determination of glycogen in small tissue samples. J Appl Physiol 1970;28:234–6.
13. Stanner MW, Mount LE, Bligh J. Energy balance and temperature regulation. Cambridge, UK: Cambridge University Press, 1984.
14. Keesey RE, Powley TL. The regulation of body weight. Annu Rev Psychol 1986;37:109–33.
15. Ballor DL, Tommerup LJ, Thomas DP, Smith DB, Keesey RE. Exercise attenuates diet-induced reduction of metabolic rate. J Appl Physiol 1990;68:2612–7.
16. Frieden E, Lipner H. Biochemical endocrinology of the vertebrates. Englewood Cliffs, NJ: Prentice-Hall, 1971:63–77.
17. Stanko RT, Robertson RJ, Spina RS, Reilly JJ Jr, Greenawalt KD, Goss FL. Enhancement of arm exercise endurance capacity with dihydroxyacetone and pyruvate. J Appl Physiol 1990;68:119–24.
18. Rogers KL, Kris-Etherton PM. The effect of weight loss and weight maintenance on high density lipoprotein cholesterol and selected tissue cholesterol levels in lean and obese Zucker rats. J Nutr 1983;113:1299–306.
19. Gerich JE, Mitrakou A, Kelly D. et al. Contribution of impaired muscle glucose clearance to reduced postabsorptive systemic glucose clearance in NIDDM. Diabetes 1990;39:211–6.
20. Stanko RT, Robertson RJ, Galbreath RW, Reilly JJ Jr, Greenawalt KD, Goss FL. Enhanced leg exercise endurance with a high-carbohydrate diet and dihydroxyacetone and pyruvate. J Appl Physiol 1990;69:1651–6.
21. Katz LD, Glickman MG, Rapoport S, Ferrannini E, DeFronzo RA. Splanchnic and peripheral disposal of oral glucose in man. Diabetes 1983;32:675–9.
22. Gutman RA, Basilico MZ, Bernal A, Chicco A, Lombardo YB. Long-term hypertriglyceridemia and glucose intolerance in rats fed chronically an isocaloric sucrose-rich diet. Metabolism 1987;36:1013–20.
23. Reiser S, Hallfrisch J. Insulin sensitivity and adipose tissue weight of rats fed starch or sucrose diets ad libitum or in meals. J Nutr 1977;107:147–50.
24. Storlien LH, Kraegen EW, Jenkins AB, Chisholm DJ. Effects of sucrose vs starch diets on in vivo insulin action, thermogenesis, and obesity in rats. Am J Clin Nutr 1988;47:420–7.
25. Wright DW, Hansen RI, Mondon CE, Reaven GM. Sucrose-induced insulin resistance in the rat: modulation by exercise and diet. Am J Clin Nutr 1983;38:879–83.

The American Journal of Clinical Nutrition

Exhibit E

Mitochondrial uncoupling protein may participate in futile cycling of pyruvate and other monocarboxylates

PETR JEŽEK AND JIŘÍ BORECKÝ
Department of Membrane Transport Biophysics, Institute of Physiology, Academy of Sciences of the Czech Republic, CZ-14220 Prague 4, Czech Republic

Ježek, Petr, and Jiří Borecký. Mitochondrial uncoupling protein may participate in futile cycling of pyruvate and other monocarboxylates. *Am. J. Physiol.* 275 (*Cell Physiol.* 44): C496–C504, 1998.—The physiological role of monocarboxylate transport in brown adipose tissue mitochondria has been reevaluated. We studied pyruvate, α-ketoisovalerate, α-ketoisocaproate, and phenylpyruvate uniport via the uncoupling protein (UCP1) as a GDP-sensitive swelling in K^+ salts induced by valinomycin or by monensin and carbonyl cyanide-*p*-(trifluoromethoxy)phenylhydrazone in Na^+ salts. We have demonstrated that this uniport is inhibited by fatty acids. GDP inhibition in K^+ salts was not abolished by an uncoupler, indicating a negligible monocarboxylic acid penetration via the lipid bilayer. In contrast, the electroneutral pyruvate uptake (swelling in ammonium pyruvate or potassium pyruvate induced by change in pH) mediated by the pyruvate carrier was inhibited by its specific inhibitor α-cyano-4-hydroxycinnamate but not by fatty acids. Moreover, α-cyano-4-hydroxycinnamate enhanced the energization of brown adipose tissue mitochondria, which was monitored fluorometrically by 2-(4-dimethylaminostyryl)-1-methylpyridinium iodide and safranin O. Consequently, we suggest that UCP1 might participate in futile cycling of unipolar ketocarboxylates under certain physiological conditions while expelling these anions from the matrix. The cycle is completed on their return via the pyruvate carrier in an H^+ symport mode.

brown adipose tissue; uncoupling protein 1; pyruvate carrier; uniport of monocarboxylates; anion futile cycling

NONSHIVERING THERMOGENESIS in newborn mammals, including humans, or in adulthood, when induced by cold adaptation or overnutrition or under specific pathological conditions, takes place in mitochondria of the brown adipose tissue (BAT) (3, 5, 9, 23, 25). BAT mitochondria generate heat due to uncoupling protein 1 (UCP1), which is specific for BAT, unlike the ubiquitous uncoupling protein 2 (6). UCP1 dissipates a protonmotive force by mediating H^+ backflow (18, 23). According to a recent hypothesis, this is carried out by a unique fatty acid cycling mechanism (7, 11, 15, 31). UCP1 is considered to conduct anionic fatty acids. Simultaneously, fatty acids are able to return in a protonated form via the lipid bilayer. The overall cycle leads to H^+ translocation (7, 31) and, hence, to uncoupling. Indeed, UCP1 can be regarded as a pure anion uniporter, strictly specific for monovalent unipolar anions (14), since it translocates their wide spectrum, alkylsulfonates, oxohalogenides, and monovalent phosphate analogs (14), including anionic forms of physiologically abundant fatty acids (7). The transport of all anions is allosterically inhibited by GDP (11) and other purine nucleotides. Thus UCP1 exhibits the widest substrate specificity among the homologous anion transporters of the mitochondrial gene family (18). For UCP1, only single charged anions and their unipolarity[1] are limiting (14).

Among mitochondrial metabolite anions (19), pyruvate has been demonstrated to be a UCP1 substrate (14). It is not trivial to ask, What is the physiological role of such monocarboxylate transport via UCP1, since a futile cycling of pyruvate might proceed in a manner similar to that of the cycling of fatty acids? The anionic monocarboxylates would be expelled from the matrix because of the negative membrane potential ($\Delta\psi$) generated by the respiratory chain, whereas their return in an H^+ symport (electroneutral) mode could proceed via specific metabolite carriers, the pyruvate or the α-ketoisovalerate carriers. Such a mechanism is plausible under the following conditions: *1*) UCP1 should provide monocarboxylate uniport, *2*) BAT mitochondria should contain carriers allowing for electroneutral uptake (H^+ symport) of monocarboxylates, the pyruvate carrier (4, 19), or the α-ketoisovalerate carrier (10), and *3*) these carriers should be active at an intermediate thermogenic state, when the anion uniport pathway of UCP1 is not completely inhibited by ATP and is not saturated by fatty acids. In this state a minimum change in pH (ΔpH) should be established to drive the pyruvate-H^+ symport. *Condition 1* is fulfilled, because a GDP-sensitive pyruvate uniport in BAT mitochondria was described previously (14). However, other unipolar ketocarboxylates were not studied, and it is not known whether fatty acids can compete with ketocarboxylates. Moreover, regulation of UCP1 activity is complex and includes variations in the levels of free fatty acids and cytosolic purine nucleotides (20). The nucleotide inhibitory ability is negatively modulated by increasing pH and Mg^{2+} (16). It has long been known that full coupling of BAT mitochondria in vitro is possible only when the fatty acids are removed (by BSA or combustion via the carnitine cycle) and, at the same time, purine nucleotides such as GDP are present (17, 26, 28). Why simple removal of the cycling agent, a fatty acid, is not sufficient to cause full coupling of BAT mitochondria has not been explained.

Condition 2 is also valid: because BAT mitochondria can respire with pyruvate (21), they exhibit an uptake of [^{14}C]pyruvate and swell in ammonium pyruvate (4). However, *condition 3* needs to be investigated, and this is the main issue of this article. We have found that, in addition to pyruvate, UCP1 also translocates other unipolar ketocarboxylates and that their transport is

[1] Unipolarity refers to a condition stating that, if there is a polar group besides the carboxyl (or other charged group), it should be located close to the carboxyl group.

0363-6143/98 $5.00

inhibited by fatty acids. The presence of the pyruvate carrier in BAT mitochondria was confirmed, and inhibition of this carrier by α-cyano-4-hydroxycinnamate (α-CHC) was shown to enhance mitochondrial energization. Hence, it is suggested that futile cycling of ketocarboxylates might partially contribute to uncoupling of mitochondria in BAT.

MATERIALS AND METHODS

Most of the chemicals were purchased from Sigma Chemical or Fluka; 2-(4-dimethylaminostyryl)-1-methylpyridinium iodide (DASMPI) was a kind gift of Prof. J. Rafael (University of Heidelberg, Heidelberg, Germany). Syrian hamsters were cold adapted for at least 3 wk at 5°C. BAT mitochondria were isolated in a medium containing 250 mM sucrose, 10 mM Tris-MOPS, 1 mM Tris-EGTA, pH 7.4, and BSA (5 mg/ml); the final washing was performed in a BSA-free medium. BSA was omitted during the isolation of mitochondria for some $\Delta\psi$ measurements.

Anion uniport indicated by osmotic swelling was measured by following the decrease in apparent absorbance given by light scattering in the 530- to 550-nm range with use of a diode-array spectrophotometer (Spectronics 3000, Milton Roy). Light-scattering intensity reflects the inverse volume (2). All media contained 0.1 mM Tris-EGTA, 2–8 μM rotenone, and 1 μM oligomycin. Passive swelling in the absence of respiration was assayed routinely in the presence of 0.25 μg/ml antimycin. Usually, 0.2 mg protein/ml of BAT mitochondria were used per assay in a medium of 40% isotonic osmolarity (270 mosmol taken as 100%), i.e., in 54 mM salts of monovalent anions buffered to pH 7.2 with 5 mM Tris-MOPS. The transport rates (in min^{-1}) were calculated as the time changes in a normalized light-scattering parameter β (2), which was calculated as follows

$$\beta = P/P_S * (A^{-1} - \alpha) \qquad (1)$$

where P is the mitochondrial concentration (mg/ml), P_S is the standard mitochondrial concentration of 1 mg/ml, A^{-1} is the inverse absorbance of the suspension, and α is a machine constant (2) equal to 0.1163 for the Spectronics 3000 diode-array spectrophotometer.

O_2 consumption of mitochondria was measured at 37°C in a 5-ml thermostatically controlled chamber equipped with a Clark polarographic electrode in a medium containing 250 mM sucrose, 10 mM Tris-MOPS, 1 mM Tris-EGTA, pH 7.4, and 40 μM rotenone. Energization (uncalibrated $\Delta\psi$) of a mitochondrial suspension was continuously monitored (17, 22, 28) in the same medium by a fluorescence probe, DASMPI (3 μM), with excitation at 467 nm and emission at 561 nm with use of 2-nm slit widths on an Ortec fluorescence spectrometer (model 9200, EG & G) or a Shimadzu fluorometer (model RF5301 PC), with excitation vertically polarized (5-nm slit width) and the emission collected through a 10-nm slit and a polarizer in cross orientation to eliminate scattering. $\Delta\psi$ was estimated according to Mewes and Rafael (22). For calibration, we assumed that under maximum energization (GDP + BSA) $\Delta\psi$ of 170 mV is established and with BSA only $\Delta\psi$ of 37.5 mV is established (26), while ΔpH is 50 mV at pH 7.2 (26) and overall protonmotive force is 220 and 87.5 mV, respectively. A net fluorescence intensity was obtained when light scattering and a fluorescence increase due to BSA interaction with the probe were taken into account. Alternatively, $\Delta\psi$ was monitored by 12.5 μM safranin, as described elsewhere (13), in the same medium in which DASMPI was used.

RESULTS

Uncoupling protein mediates uniport of monovalent ketocarboxylates. In accordance with our previous observations and conclusions (14), we reevaluated the ability of UCP1 to conduct physiologically relevant "metabolic" anions. We studied valinomycin-induced uptake of K^+ salts of pyruvate (Fig. 1*A*) and phenylpyruvate (Fig. 1*B*) in nonrespiring BAT mitochondria pretreated with BSA. An inhibitor of the pyruvate carrier (27), α-CHC, was routinely present to eliminate the pyruvate

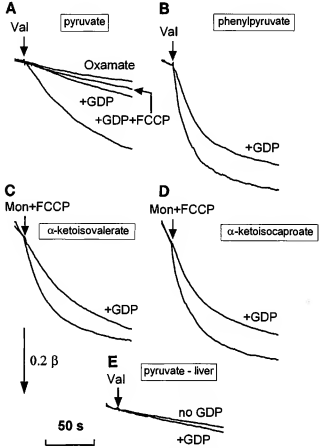

Fig. 1. Uniport of pyruvate and other unipolar ketocarboxylates via uncoupling protein in brown adipose tissue (BAT) mitochondria (*A–D*) and its absence in liver mitochondria (*E*). Uniport of pyruvate (*A*), phenylpyruvate (*B*), α-ketoisovalerate (*C*), and α-ketoisocaproate (*D*) was measured as a passive swelling monitored by light scattering. Swelling was induced by 1 μM valinomycin (Val) in 55 mM K^+ salts buffered to pH 7.2 with 5 mM Tris-MOPS (*A* and *B*) or by a mixture of 1 μM monensin (Mon) and 1 μM carbonyl cyanide-*p*-(trifluoromethoxy)phenylhydrazone (FCCP) in 55 mM Na^+ salts (*C* and *D*) and 5 mM Tris-MOPS, pH 7.2, all in presence of 1 mM α-cyano-4-hydroxycinnamate (α-CHC). +GDP and +GDP + FCCP, traces measured with 1 mM GDP and with 1 mM GDP and 1 μM FCCP, respectively; oxamate, trace measured in K^+ salt of oxamate (β-amino-α-ketoacetate). All assays contained 0.1 mM Tris-EGTA, 2 μM rotenone, 0.25 μg/ml antimycin, and 0.2 mg protein/ml of BAT or liver mitochondria.

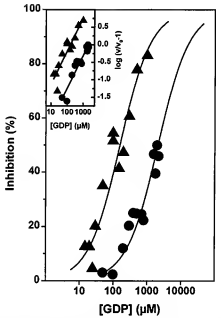

Fig. 2. Dose responses for inhibition of pyruvate and phenylpyruvate uniport via uncoupling protein 1 (UCP1) by GDP. GDP dose responses for pyruvate (▲) and phenylpyruvate (●) uniport were constructed from titrations by GDP. Measurements were performed under conditions described in Fig. 1 legend. Inhibitory ability in percent is expressed as 100% (v_0) minus remaining activity in percent at given GDP dose (v). Curves were drawn on assumption that infinite GDP would yield 100% inhibition. Dose responses were fitted on basis of linearization of Hill plots (*inset*), and fits were drawn according to Hill's equation (solid lines). This procedure yielded Hill's coefficient (n_H) of 0.95 for pyruvate and phenylpyruvate and inhibition constants (K_i) of 155 and 2,076 μM, respectively.

carrier-mediated flux. The pyruvate uptake was highly sensitive to GDP (Figs. 1 and 2), and the inhibition was not released by carbonyl cyanide-*p*-(trifluoromethoxy) phenylhydrazone (FCCP; Fig. 1*A*). This excludes the possibility that monocarboxylates pass through the membrane as neutral acids and that UCP1 participates only in H^+ reentry.[2] Hence, the observed GDP-sensitive fluxes must be ascribed to the function of UCP1. This is also confirmed by the absence of valinomycin-induced swelling of rat liver mitochondria in potassium pyruvate in the presence of α-CHC (Fig. 1*E*).

Typical rates of UCP1-mediated transport were 0.2 and 1.0 min^{-1} in pyruvate and phenylpyruvate, respectively. For comparison, the rate in a Cl^- medium was 0.3 min^{-1} (not shown). UCP1 also translocates α-ketoisovalerate (Fig. 1*C*) and α-ketoisocaproate (Fig. 1*D*), as demonstrated by GDP-sensitive swelling induced by monensin in the Na^+ salts in the presence of FCCP. The typical rates reached 0.6 and 0.7 min^{-1}, respectively. GDP (1 mM) caused incomplete inhibition in Fig. 1, *B–D*. This is due in part to an apparently lower affinity for GDP in inhibiting these anions (see below). All monocarboxylate substrates tested always have a second polar (carbonyl) group near the carboxyl. When this unipolarity requirement is not fulfilled (14) or when a third polar group is attached, as in the case of oxamate (β-amino-α-ketoacetate, Fig. 1*A*), then the anion is not translocated by UCP1.

GDP inhibition of transport of various UCP1 anionic substrates was previously found to exhibit different inhibition constants (K_i). Particularly, K_i values increased with the increasing hydrophobicity or size of anions (14). This phenomenon is probably due to interference of hydrophobic anions with GDP binding, as demonstrated by Nedergaard and Cannon (24) in the case of benzenesulfonate. We evaluated the K_i values for GDP inhibition of uniport of all four carboxylates shown in Fig. 1 at pH 7.2, and two representative dose-response curves are illustrated in Fig. 2. The curves were drawn on the assumption that infinite GDP would yield 100% inhibition, and K_i values were derived from the Hill plots (Fig. 2, *inset*). Indeed, K_i increased with increasing hydrophobicity. K_i for inhibition of pyruvate uniport was 155 μM, whereas K_i values for the more hydrophobic carboxylates were between 1 mM (α-ketoisovalerate) and 2 mM (phenylpyruvate and α-ketoisocaproate).

Fatty acids and monocarboxylates share the same pathway in UCP1. The mutual competition of fatty acids and other anionic substrates on UCP1 has repeatedly been reported (7, 11, 15, 29). Because some artificial derivatives such as azido fatty acid, 12-(4-azido-2-nitrophenylamino)dodecanoic acid (AzDA), were previously shown to inhibit Cl^- uniport via UCP1 more potently than natural fatty acids (15), we investigated whether the UCP1-mediated pyruvate uniport is also inhibited by AzDA. Figure 3 shows strong inhibition by 40 μM AzDA in the dark (i.e., not photoactivated),[3]

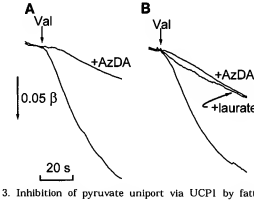

Fig. 3. Inhibition of pyruvate uniport via UCP1 by fatty acids. Valinomycin-induced passive swelling of BAT mitochondria in potassium pyruvate was measured in absence (*A*) and presence (*B*) of 1 mM α-CHC. Effect of 500 μM lauric acid (+laurate) and 40 μM 12-(4-azido-2-nitrophenylamino)dodecanoic acid (+AzDA) was studied. Rates were 0.25 and 0.045 min^{-1} in control and with AzDA (82% inhibition) in *A* and 0.23, 0.053, and 0.048 min^{-1} in control and with lauric acid (77% inhibition) and AzDA (79% inhibition), respectively, in *B* with α-CHC. See Fig. 1 legend for other details.

[2] H^+ transport mediated by UCP1 is most probably a result of fatty acid cycling (6). Residual endogenous fatty acids that were not removed by BSA treatment could therefore provide such an H^+-conducting pathway.

independently of the presence of α-CHC. A similar result was also obtained with lauric acid, a natural fatty acid, but at a much higher concentration of 500 μM (Fig. 3*B*, +laurate). As a gauge for nonspecific changes that could be caused by AzDA and lauric acid, we tested swelling in potassium acetate with nigericin, which acts independently of a protein carrier (not shown). This swelling was not affected by concentrations of up to 50 μM with AzDA or up to 500 μM with lauric acid. Figure 4 illustrates the dose responses for inhibition of pyruvate uniport by AzDA and lauric acid. Apparent K_i was ~10 μM, irrespective of whether α-CHC was present. The inhibitory effect of lauric acid was lower (K_i = 306 μM). Similar data were found for other monocarboxylates (not shown).

Pyruvate carrier in BAT mitochondria is inhibited by α-CHC but not by fatty acids. A symport of H^+ and monocarboxylates can be provided in mitochondria by the pyruvate and the α-ketoisovalerate carrier (10, 19). The former has been assumed to allow for respiration of BAT mitochondria with pyruvate (21). Therefore, our further goal was to reevaluate a non-UCP1-mediated electroneutral pyruvate uptake in BAT mitochondria that can be ascribed to the pyruvate carrier. For this purpose, we first studied the swelling of BAT mitochondria in ammonium pyruvate (Fig. 5). The pyruvate uptake representing such swelling (4) must be electroneutral, proceeding as a symport with H^+, since only the neutral NH_3 is able to pass through the membrane. The transport was inhibited by α-CHC with a K_i of 5.5 mM (Fig. 5*C*). On the contrary, it was not inhibited by AzDA (Fig. 4) or by lauric acid. The electroneutral nigericin-induced uptake of pyruvate in the presence of GDP and the absence of α-CHC was quite slow in nonrespiring BAT mitochondria (0.05 min^{-1}) as well as its α-CHC-sensitive part (0.03 min^{-1}, Fig. 5*A*). This shows that the activity of the pyruvate carrier is low under these conditions. However, another electroneutral transport induced by nigericin, a phosphate-H^+ symport via the phosphate carrier, was not obstructed, as shown in a parallel experiment (Fig. 5*A*).

We have also developed a new assay for electroneutral pyruvate transport in which we employ the valinomycin-induced swelling in potassium pyruvate under conditions when fully coupled BAT mitochondria (by GDP and BSA) are respiring with α-glycerophosphate (Fig. 6). Propranolol was also present to exclude most of the inner membrane anion channel-mediated flux (1). Under these conditions, respiratory H^+ pumping compensates the pyruvate-H^+ symport and the simultaneous K^+ uniport (influx). Moreover, addition of valinomycin to coupled mitochondria is known to create an initial ΔpH jump (1). Thus ΔpH drives the pyruvate-H^+ symport. As demonstrated in Fig. 6, such electroneutral pyruvate-H^+ symport was sensitive to α-CHC with a K_i of 9 mM (Fig. 5*C*), indicating the participation of the pyruvate carrier. Similar results were obtained with

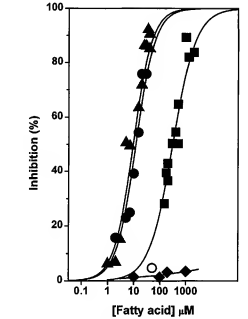

Fig. 4. Dose responses for fatty acid inhibition of pyruvate uniport via UCP1 and lack of fatty acid inhibition of pyruvate carrier. Dose responses for AzDA inhibition were measured in presence (●) and absence (▲) of 1 mM α-CHC and for lauric acid inhibition (■) of pyruvate uniport via UCP1. Lack of inhibition by AzDA of pyruvate carrier-mediated electroneutral pyruvate-H^+ symport is also illustrated when assay was assessed as swelling in ammonium pyruvate (♦, see Fig. 5 legend) or as ΔpH-induced swelling (○, see Fig. 6 legend). Inhibitory ability is expressed as 100% minus remaining activity in percent at a given AzDA dose. Theoretical curves (solid lines) were fitted using linearization of Hill plots (not shown) and drawn on basis of Hill's equation with assumption that infinite AzDA (lauric acid) would yield 100% inhibition. For AzDA, n_H was 1.2 with 1 mM α-CHC and without α-CHC and K_i was 11.3 and 9.3 μM, respectively. For lauric acid, n_H was 0.98 and K_i was 306 μM. See Fig. 1 legend for other details.

the other known substrates of the pyruvate carrier such as phenylpyruvate (Fig. 6*B*), lactate (Fig. 6*C*), and chloroacetate (Fig. 6*D*). The residual inhibitor-insensitive portion could be attributed to the nonionic diffusion of pyruvic and other ketocarboxylic acids across the lipid bilayer or to the uninhibited part of the inner membrane anion channel-mediated flux. A contribution of the former process should be minor, as documented by the very slow passive swelling of BAT mitochondria in potassium pyruvate in the presence of nigericin and α-CHC (Fig. 5*A*).

Effect of α-CHC on coupling of BAT mitochondria. It is well known (17, 26, 28) that addition of GDP to fatty acid-depleted BAT mitochondria leads to their maximum coupling (Δψ of 170 mV) (26). Here we demonstrate that addition of α-CHC to fatty acid-depleted BAT mitochondria leads to some coupling (Fig. 7). Monitoring Δψ fluorometrically by DASMPI (22), we found that a nearly uncoupled state of fatty acid-depleted BAT mitochondria in the absence of GDP can be further coupled by α-CHC in the presence of endogenous (not shown) or externally added pyruvate (Fig. 7). This intermediate coupling with α-CHC and BSA

[3] Photoactivated AzDA inhibited UCP1 more strongly (cf. Ref. 15).

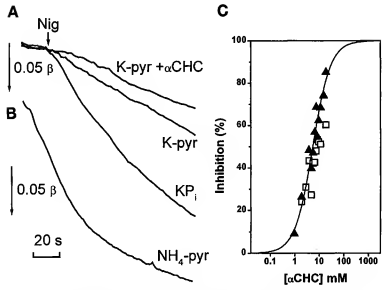

Fig. 5. *A* and *B*: pyruvate carrier function as assessed by passive swelling. Two assays for pyruvate carrier based on passive swelling were tested. *1*) Swelling was assessed in ammonium pyruvate (B, NH_4-pyr), with no nigericin (Nig) added. This assay was conducted by mixing BAT mitochondria with a medium of 54 mM ammonium pyruvate, 5 mM Tris-MOPS, and 0.1 mM Tris-EGTA, pH 7.2, containing 0.5 μg/ml antimycin, 4 μM rotenone, and 1 μM oligomycin. *2*) Passive swelling of BAT mitochondria was assessed in potassium pyruvate containing 1 mM GDP (A, K-pyr) induced by 0.13 μM nigericin in absence or presence of 1 mM α-CHC (+α-CHC), which was quite slow (rates reached 0.05 and 0.02 min^{-1}, respectively). To verify that nonrespiring BAT mitochondria possess ability to conduct an electroneutral transport in presence of 0.13 μM nigericin, a P_i-H^+ symport mediated by the P_i carrier was tested (A, KP_i) by passive swelling in KP_i (44 mM, pH 7.2). Other conditions were as for potassium pyruvate. *C*: dose response for α-CHC inhibition of pyruvate carrier. Pyruvate carrier was assayed as swelling in ammonium pyruvate (▲, cf. *B*) or ΔpH-induced swelling (□, see Fig. 6). Percent inhibitory ability was calculated as described in Fig. 4 legend. Solid line, corresponding fit of data for passive swelling by use of Hill's equation; n_H was 1.2 and K_i was 5.5 mM. For ΔpH-induced swelling (fit not shown) n_H was 1 and K_i was 9 mM.

was estimated to reach 112–135 mV (the maximum $\Delta\psi$ and the sole BSA-induced energization served as the 2 calibration points). We have explained this as a result of the elimination of pyruvate cycling. α-CHC enhanced the energization, independently of whether it was added before (not shown) or after BSA (Fig. 7*A*) or before (Fig. 7*B*) or after (Fig. 7*A*) the respiratory substrate α-glycerophosphate. Pyruvate served only as a cofactor of the putative pyruvate cycling, since rotenone was always present. Figure 7*B* shows that the energization in the presence of pyruvate and rotenone was higher with than without α-CHC. A sole pyruvate addition rather led to a slight uncoupling (Fig. 7*B*, only pyr). We have also verified that α-CHC added after FCCP did not cause any effect, nor did it interfere with the fluorescence of DASMPI (not shown). We have also confirmed the well-known fact (17, 26, 28) that the sole addition of GDP (not shown) or sole fatty acid removal (Fig. 7) did not lead to complete coupling, but only to small $\Delta\psi$. Also, GDP added after α-CHC was still able to induce maximum energization (Fig. 7*A*, dashed trace). Note that the scale in millivolts is nonlinear with regard to the fluorescence; consequently, this energization appears to be exaggerated.

Parallel measurements of respiration by a Clark O_2 probe confirmed that the α-CHC-induced coupling decreases O_2 consumption of BAT mitochondria, whereas the addition of an uncoupler accelerates their respiration (Fig. 7*C*). Rat liver mitochondria respiring with endogenous substrates (i.e., without rotenone, Fig. 8*A*) or nonenergized (with rotenone), in the presence (Fig. 8*A*, *bottom trace*) or absence of pyruvate (Fig. 8*B*), exhibited no increase in $\Delta\psi$ after addition of α-CHC. Instead, a slight decrease of $\Delta\psi$ was noted. Succinate, when added after α-CHC, was still able to energize rat liver mitochondria to a maximum coupling (Fig. 8*B*).

The alternative monitoring of $\Delta\psi$ by safranin also confirmed the coupling effect of α-CHC in BAT mitochondria (Fig. 9). In contrast to DASMPI, safranin fluorescence is quenched with increasing $\Delta\psi$, so one could expect almost "mirror" changes in the fluorescence records, and this was indeed the case. α-CHC enhanced the energization independently of whether added after BSA (Fig. 9*A*) or before BSA (Fig. 9. *B* and *C*). The latter effect of α-CHC was higher in the presence of externally added pyruvate (Fig. 9, *B* vs. *C*). As expected, ATP added after BSA induced the maximum energization (Fig. 9, *B* and *C*). These results again suggest that the inhibition of the pyruvate carrier may eliminate pyruvate cycling, in which this carrier participates with UCP1.

DISCUSSION

Jeżek and Garlid (14) reported for the first time that UCP1 can translocate pyruvate and acetate. We have now extended these findings to the entire class of

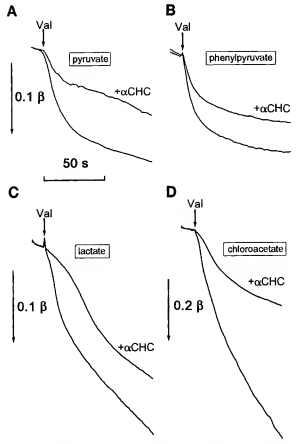

Fig. 6. ΔpH-induced swelling of monocarboxylates mediated by pyruvate carrier in BAT mitochondria. Transport of pyruvate (*A*), phenylpyruvate (*B*), lactate (*C*), and chloroacetate (*D*) was measured in respiring coupled BAT mitochondria in presence of 1 mM GDP and BSA (1.5 mg/ml) and 5 mM α-glycerophosphate in media containing 5 mM Tris-MOPS, pH 7.2, and 1 mM Tris-EGTA in absence of antimycin as a ΔpH-induced swelling initiated by 1 μM valinomycin. Valinomycin is known (cf. Ref. 1) to create a ΔpH jump in respiring coupled mitochondria. ΔpH then drives a monocarboxylate-H^+ symport. Inhibition by 1 mM α-CHC (+α-CHC) indicates participation of pyruvate carrier. Other conditions were similar to those described in Fig. 1 legend.

unipolar ketocarboxylates. Our data show that UCP1 allows for the uniport of phenylpyruvate, α-ketoisovalerate, and α-ketoisocaproate, which have not been identified as the UCP1 substrates. We can also suggest that fatty acids and unipolar monocarboxylates compete within a single pathway of the UCP1. A model fatty acid, AzDA (15, 29, 30), and the natural lauric acid inhibit the uniport of pyruvate via UCP1, but not electroneutral pyruvate transport, mediated by the pyruvate carrier. The latter was clearly identified in BAT mitochondria, and its inhibition by α-CHC resulted in an increased coupling of BAT mitochondria (which was incomplete). Our data suggest that, even in the absence of fatty acids, futile cycling of pyruvate and other monocarboxylate anions might mimic the fatty acid cycling uncoupling mechanism (7, 31). All monovalent anions, which may enter into the matrix by a symport with H^+, could be involved. This could be ensured by the pyruvate carrier or by the α-ketoisovalerate carrier. Hence, the existence of the futile cycling of monocarboxylates could contribute, at least partially, to the uncoupling and enable a fine regulation of coupling in BAT mitochondria (Fig. 10).

Features of the uncoupling protein. The UCP1 is now a well-characterized uniporter of monovalent anions. Striking analogy between the character and size of fatty acids and UCP1 amphiphilic substrates such as alkylsulfonates [translocation of which was directly proven (7, 14)] and the mutual competition of fatty acids and alkylsulfonates (7, 11, 15, 29) supports the fatty acid cycling mechanism (7). We now suggest that not only can long-chain fatty acids undergo such cycling but also the compounds with a short chain, namely, the monocarboxylic α-ketoacids (Fig. 10). We have unambiguously characterized pyruvate and other unipolar ketocarboxylates as the transport substrates of UCP1. We may assume that maximal reaction velocity (V_{max}) for pyruvate uniport via UCP1 will be close to the value found for Cl^- uniport (7) and that the Michaelis-Menten constant is on the order of 10 mM. Even if V_{max} is lower and the assumed affinity (the inverse Michaelis-Menten constant) is much lower than the corresponding parameters for the fatty acid uniport, pyruvate uniport in the absence of fatty acids would still be able to contribute to the uncoupling at a pyruvate physiological concentration of 0.1 mM (10). Under these conditions, 1% of V_{max} amounts to 100 nmol $H^+ \cdot min^{-1} \cdot mg$ $UCP1^{-1}$, which is equal to the turnover of 7 s^{-1}. Because it is known that free Mg^{2+} also prevents nucleotide inhibition of anion uniport via UCP1, we can expect that at least 35% of in vitro measured pyruvate uniport activity will remain (16) at the physiological concentrations of Mg^{2+} and ATP, 0.5 mM in a thermogenic state (20).

The ketocarboxylate uniport via UCP1 is presumably competitively inhibited by fatty acids (Figs. 3 and 4) and allosterically (11) by GDP (Figs. 1 and 2). With unipolar ketocarboxylates, we confirmed both trends, which were previously revealed for the UCP1-substrate pattern, namely, that the transport rates are enhanced with increasing hydrophobicity of the anion (14), e.g., phenylpyruvate vs. pyruvate. A second feature, that GDP inhibition of anion uniport is decreasing with the hydrophobicity of the anion (with increasing K_i), was also confirmed for ketocarboxylates. Moreover, residual GDP-insensitive transport in Na^+ salts of α-ketoisovalerate and α-ketoisocaproate might indicate that BAT mitochondria contain a branched-chain α-ketoacid carrier (10).

Regulation of thermogenesis in BAT. Regulation of thermogenesis in BAT has not yet been satisfactorily explained. A central mechanism should involve a single third messenger (or several such messengers) between norepinephrine-stimulated cAMP levels and UCP1 (23). The most plausible candidate according to LaNoue et al. (20) is ATP, which drops to 0.5 mM in thermogenic BAT cells. At physiological free Mg^{2+} concentrations and pH, this ATP level is not inhibitory and allows the UCP1 transport pathway to open (16). At the same

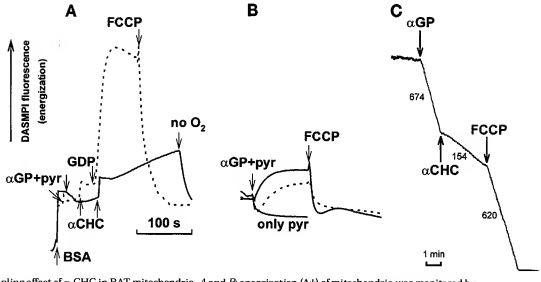

Fig. 7. Coupling effect of α-CHC in BAT mitochondria. *A* and *B*: energization ($\Delta\psi$) of mitochondria was monitored by increasing fluorescence of 6 μM 2-(4-dimethylaminostyryl)-1-methylpyridinium iodide (DASMPI), added at beginning of each trace. BAT mitochondria were resuspended to 1 mg protein/ml in an O_2-saturated medium containing 250 mM sucrose, 10 mM Tris-MOPS, 1 mM Tris-EGTA, pH 7.4, and 40 μM rotenone. *A*: BAT mitochondria containing natural endogenous fatty acids. Solid trace, effect of α-CHC added after α-glycerophosphate (α-GP) and pyruvate. First, BSA (5 mg/ml) was added to eliminate fatty acids; corresponding fluorescence increase is mostly due to BSA interaction with DASMPI. Subsequently, a substrate, 10 mM α-glycerophosphate, Na^+ salt, and a cofactor, 5 mM Tris-pyruvate, were added (arrow, α-GP + pyr), causing a slight signal decrease. Addition of 1 mM α-CHC caused a biphasic fluorescence ($\Delta\psi$) increase, which was terminated by anoxia (no O_2). Dashed trace, coupling effect of 1 mM GDP added after 1 mM α-CHC. Order of additions before GDP was as described above. A complete uncoupling induced by 2 μM FCCP is also demonstrated; fluorescence ($\Delta\psi$) dropped to original low value. *B*: BAT mitochondria were isolated with BSA, which was also present in assay medium (5 mg BSA/ml). *Top trace*, α-CHC effect when 1 mM α-CHC was added before α-glycerophosphate and pyruvate (α-GP + pyr). Because 40 μM rotenone was present, only former represents a respiratory substrate. This is compared with same measurement without α-CHC (dashed trace) and without both α-CHC and α-glycerophosphate (*bottom trace*, only pyr). *C*: α-CHC-induced coupling of BAT mitochondria monitored by O_2 consumption. BAT mitochondria (0.4 mg protein/ml) were injected into a 5-ml chamber with a Clark polarographic O_2 probe containing an O_2-saturated medium of same composition used for $\Delta\psi$ monitoring, supplemented by 7.5 mg BSA/ml. As indicated by arrows, 10 mM Tris-pyruvate (pyr), 4 mM α-glycerophosphate, Na^+ salt (α-GP), 8 mM α-CHC, and 4 μM FCCP were added. Numbers under trace are respiratory rates in nmol $O \cdot min^{-1} \cdot mg\ protein^{-1}$.

time, fatty acid levels are elevated, and this leads to the thermogenic state.

We may hypothesize that the sole removal (combustion) of fatty acids can arrest the uncoupling cycle of fatty acids but not of monocarboxylates. The latter would be blocked only when high levels of ATP or other purine nucleotides are also present. Thus, in the absence of fatty acids as cycling agents, pyruvate cycling

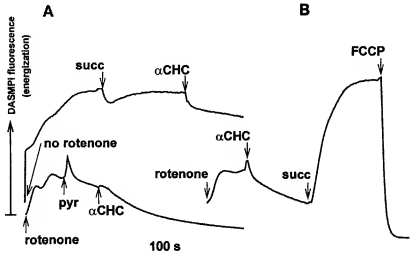

Fig. 8. Lack of α-CHC effect in rat liver mitochondria. Energization ($\Delta\psi$) of rat liver mitochondria (1 mg protein/ml) was monitored by increasing fluorescence of DASMPI as described in Fig. 7 legend. In *A*, 1 mM α-CHC was added to mitochondria energized almost completely by endogenous substrates [no rotenone, *top trace*; note that 10 mM Tris-succinate (succ) did not further increase $\Delta\psi$] or to nonenergized mitochondria (*bottom trace*), where effect of 5 mM Tris-pyruvate was also evaluated (pyr). In *B*, 10 mM succinate (succ) added after α-CHC was still able to induce maximum coupling; uncoupling induced by 2 μM FCCP is illustrated as well.

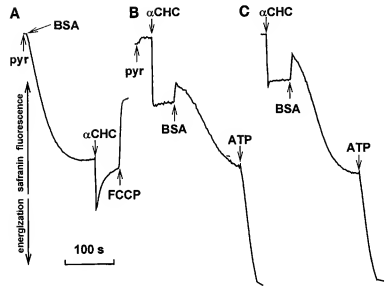

Fig. 9. Monitoring α-CHC effect in BAT mitochondria by safranin. Energization ($\Delta\psi$) of BAT mitochondria (1 mg/ml) partially depleted of fatty acids was monitored by decreasing fluorescence of 12.5 μM safranin in an O_2-saturated medium containing 250 mM sucrose, 10 mM Tris-MOPS, 1 mM Tris-EGTA, pH 7.4, 10 mM α-glycerophosphate, Na^+ salt, and 40 μM rotenone. *Traces A* and *B* were mutated with 5 mM Tris-pyruvate and *trace C* without pyruvate. α-CHC (1 mM), added after (*A*) or before (*B* and *C*) BSA enhanced $\Delta\psi$. Increase in $\Delta\psi$ was higher in presence of 5 mM Tris-pyruvate (*B* vs. *C*). Addition of BSA and ATP led to further coupling, whereas 2 μM FCCP led to uncoupling, despite a signal shift due to addition of BSA.

may play an important regulatory role for thermogenesis, when fatty acids are rapidly depleted from the triglyceride droplets. Our current data support this point of view. Despite the fact that α-CHC in fatty acid-depleted BAT mitochondria does not induce the highest coupled state, the observed partial $\Delta\psi$ increase is sufficient for delicate regulation of coupling. This partial $\Delta\psi$ increase can be interpreted as a result of blockage of pyruvate cycling by inhibition of pyruvate uptake via the pyruvate carrier.

Features of the pyruvate carrier in BAT mitochondria. The presence of the pyruvate carrier in BAT mitochondria has previously been indicated by the high capacity of BAT mitochondria (21) and BAT cells (25) to oxidize pyruvate as a respiratory substrate by the existence of swelling of BAT mitochondria in ammonium pyruvate and by the respiratory-driven uptake of [^{14}C]pyruvate into BAT mitochondria (4). We have confirmed the existence of swelling in ammonium pyruvate, and we have demonstrated the respiratory-driven ΔpH-induced electroneutral transport of pyruvate and other monocarboxylates in BAT mitochondria. Both processes are sensitive to α-CHC, a specific inhibitor of the pyruvate carrier (27), but are insensitive to fatty acids (Fig. 4). The former is driven by NH_3 permeation into the membrane, and subsequent matrix alkalinization results from the formation of NH_4^+, whereas the latter process is driven by ΔpH of the same orientation, i.e., by the increased ΔpH under conditions when K^+ uptake by valinomycin discharges the $\Delta\psi$ component of the proton electrochemical gradient ($\Delta\tilde{\mu}_{H^+}$). Swelling in ammonium pyruvate is fast (4), because a much greater NH_4^+ gradient is established and concomitant matrix alkalinization creates ΔpH comparable in magnitude to that during respiration.

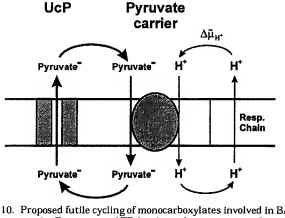

Fig. 10. Proposed futile cycling of monocarboxylates involved in BAT thermogenesis. Decrease in ATP level results in opening of uncoupling protein (UCP) for pyruvate efflux. Pyruvate might return together with an H^+ on pyruvate carrier, thus completing uncoupling cycle. Uncoupling decreases electrochemical proton gradient ($\Delta\tilde{\mu}_{H^+}$).

Slow electroneutral pyruvate transport was detected only when we attempted to induce passive swelling of BAT mitochondria in potassium pyruvate by nigericin in the presence of GDP. First, it shows that pyruvate, unlike acetate, is poorly permeant through the mitochondrial membrane itself. Otherwise, swelling in potassium pyruvate and nigericin should be as rapid as any swelling independent of a protein carrier. Because during a passive swelling nigericin collapses ΔpH, we might conclude that electroneutral pyruvate transport is slow at low ΔpH. This has been suggested also for the dicarboxylate carrier (12). Such a ΔpH regulation would represent a rate-limiting step in pyruvate cycling. Consequently, pyruvate cycling is expected to be a fine regulatory mechanism rather than a major thermogenic mechanism.

In conclusion, pyruvate (monocarboxylate) cycling might contribute only partially to the overall thermogenesis but should play an important role in the fine control of coupling. This could be exerted even by sequential fluxes via the pyruvate carrier and UCP1. Because of the limited penetration of pyruvic acid via the lipid bilayer, pyruvate cycling cannot proceed as

freely as fatty acid cycling but is regulated on both proteins involved. With a partially inhibited pyruvate carrier (by low ΔpH), such cycling will play only a minor role. However, on combustion of fatty acids and concomitantly enhanced $\Delta\psi$ and ΔpH, the activated pyruvate carrier will enable the pyruvate cycling in concert with the open UCP1 pathway (unsaturated with nucleotides and fatty acids).

The use of a fluorometer provided by Drs. Martin Nikl and Karel Polák (Institute of Physics, Prague, Czech Republic) is gratefully acknowledged.

This work was partly supported by Academy of Sciences of the Czech Republic Grant 51151 and later by Grant Agency of the Czech Republic Grants 301/95/0620 and 301/98/0568 and by ÚS-Czechoslovak Science and Technology Program Grant 94043, which aided the purchase of a new fluorometer.

Address for reprint requests: P. Ježek, Dept. of Membrane Transport Biophysics (No. 375), Institute of Physiology, Academy of Sciences of the Czech Republic, Vídeňská 1083, CZ-14220 Prague 4, Czech Republic.

Received 26 February 1996; accepted in final form 15 April 1998.

REFERENCES

1. **Beavis, A. D.** Properties of the inner membrane anion channel in intact mitochondria. *J. Bioenerg. Biomembr.* 24: 77–90, 1992.
2. **Beavis, A. D., R. D. Brannan, and K. D. Garlid.** Swelling and contraction of the mitochondrial matrix. I. Structural interpretation of the relationship between light scattering and matrix volume. *J. Biol. Chem.* 260: 13424–13433, 1985.
3. **Cannon, B., T. Bengtsson, A. Dicker, A. Jacobsson, P. Kuusela, H. Thornberg, P. Tvrdik, J. Zhao, and J. Nedergaard.** The role of adrenergic stimulation in regulation of heat production and recruitment of brown adipose tissue. In: *Thermal Balances in Heat and Disease, Advances in Pharmacological Sciences*, edited by E. Zeisberger, E. Schoenbaum, and P. Lomax. Basel: Birkhauser Verlag, 1994, p. 87–102.
4. **Cannon, B., V. S. M. Bernson, and J. Nedergaard.** Metabolic consequences of limited substrate anion permeability in brown fat mitochondria from a hibernator, the golden hamster. *Biochim. Biophys. Acta* 766: 483–491, 1984.
5. **Cannon, B., and J. Nedergaard.** Brown adipose tissue: molecular mechanism controlling activity and thermogenesis. In: *New Perspectives in Adipose Tissue: Structure, Function and Development*, edited by A. Cryer and R. L. R. Van. London: Butterworths, 1985, p. 223–270.
6. **Fleury, C., M. Neverova, S. Collins, S. Raimbault, O. Champigny, C. Levi-Meyrueis, F. Bouillaud, M. F. Seldin, R. S. Surwit, D. Ricquier, and C. H. Warden.** Uncoupling protein-2: a novel gene linked to obesity and hyperinsulinemia. *Nature Genet.* 15: 269–272, 1997.
7. **Garlid, K. D., D. E. Orosz, M. Modrianský, S. Vassanelli, and P. Ježek.** On the mechanism of fatty acid-induced proton transport by mitochondrial uncoupling protein. *J. Biol. Chem.* 271: 2615–2702, 1996.
8. **Heaton, G. M., and D. G. Nicholls.** Hamster brown adipose tissue mitochondria. The role of fatty acids in the control of the proton conductance of the inner membrane. *Eur. J. Biochem.* 67: 511–517, 1976.
9. **Himms-Hagen, J.** Brown adipose tissue thermogenesis: interdisciplinary studies. *FASEB J.* 4: 2890–2898, 1990.
10. **Hutson, S. M., and S. L. Rannels.** Characterization of a mitochondrial transport system for branched-chain α-keto acids. *J. Biol.Chem.* 260: 14189–14193, 1985.
11. **Ježek, P., M. Bauer, and W. E. Trommer.** EPR spectroscopy of 5-DOXYL-stearic acid bound to the mitochondrial uncoupling protein reveals its competitive displacement by alkylsulfonates in the channel and allosteric displacement by ATP. *FEBS Lett.* 361: 303–307, 1995.
12. **Ježek, P., and J. Borecký.** Inner membrane anion channel and dicarboxylate carrier in brown adipose tissue mitochondria. *Int. J. Biochem. Cell. Biol.* 28: 659–666, 1996.
13. **Ježek, P., A. D. T. Costa, and A. E. Vercesi.** Evidence for anion-translocating plant uncoupling mitochondrial protein in potato mitochondria. *J. Biol. Chem.* 271: 32743–32749, 1996.
14. **Ježek, P., and K. D. Garlid.** New substrates and competitive inhibitors of the Cl^- translocating pathway of the uncoupling protein of brown adipose tissue mitochondria. *J. Biol. Chem.* 265: 19303–19311, 1990.
15. **Ježek, P., J. Hanuš, C. Semrad, and K. D. Garlid.** Photoactivated azido fatty acid irreversibly inhibits anion and proton transport through the mitochondrial uncoupling protein. *J. Biol. Chem.* 271: 6199–6205, 1996.
16. **Ježek, P., J. Houštěk, and Z. Drahota.** Alkaline pH, membrane potential and magnesium cations are negative modulators of purine nucleotide inhibition of H^+ and Cl^- transport through the uncoupling protein of brown adipose tissue mitochondria. *J. Bioenerg. Biomembr.* 20: 603–622, 1988.
17. **Ježek, P., I. P. Krasinskaya, I. Smirnova, and Z. Drahota.** Carnitine cycle in brown adipose tissue mitochondria as a tool for studying the regulatory role of fatty acids in the uncoupling protein function. *FEBS Lett.* 243: 37–40, 1989.
18. **Klingenberg, M.** Mechanism and evolution of the uncoupling protein of brown adipose tissue. *Trends Biochem. Sci.* 15: 108–112, 1990.
19. **LaNoue, K. F., and A. C. Schoolwerth.** Metabolite transport in mitochondria. *Annu. Rev. Biochem.* 48: 871–922, 1979.
20. **LaNoue, K. F., T. Strzelecki, D. Strzelecka, and C. Koch.** Regulation of the uncoupling protein in brown adipose tissue. *J. Biol. Chem.* 251: 298–306, 1986.
21. **Locke, R. M., E. Rial, I. D. Scott, and D. G. Nicholls.** Fatty acids as acute regulators of the proton conductance of hamster brown fat mitochondria. *Eur. J. Biochem.* 129: 373–380, 1982.
22. **Mewes, H.-W., and J. Rafael.** The 2-(dimethylaminostyryl)-1-methylpyridinium cation as indicator of the mitochondrial membrane potential. *FEBS Lett.* 131: 7–10, 1981.
23. **Nedergaard, J., and B. Cannon.** The uncoupling protein thermogenin and mitochondrial thermogenesis. In: *New Comprehensive Biochemistry: Molecular Mechanisms in Bioenergetics*, edited by L. Ernster. Amsterdam: Elsevier, 1992, vol. 23, p. 385–420.
24. **Nedergaard, J., and B. Cannon.** Sulfonates are low-affinity ligands for the GDP-binding site of brown-fat mitochondria. *Biochim. Biophys. Acta* 1185: 311–317, 1994.
25. **Nedergaard, J., and O. Lindberg.** The brown fat cell. *Int. Rev. Cytol.* 74: 187–290, 1981.
26. **Nicholls, D. G.** Hamster brown adipose tissue mitochondria. The control of respiration and the proton electrochemical potential gradient by possible physiological effectors of the proton conductance of inner membrane. *Eur. J. Biochem.* 49: 573–583, 1974.
27. **Paradies, G.** Interaction of α-cyano-[^{14}C]cinnamate with the mitochondrial pyruvate translocator. *Biochim. Biophys. Acta* 766: 446–450, 1984.
28. **Rafael, J.** 2-(Dimethylaminostyryl)-1-ethylpyridinium iodide: a fluorescent probe of energetics conditions in brown adipose tissue mitochondria. *Hoppe Seylers Z. Physiol. Chem.* 361: 437–444, 1980.
29. **Růžička, M., J. Borecký, J. Hanuš, and P. Ježek.** Photoaffinity labelling of the mitochondrial uncoupling protein by ^{3}H-azido-fatty acid affects the anion channel. *FEBS Lett.* 382: 239–243, 1996.
30. **Schönfeld, P., P. Ježek, J. Borecký, E. Belyaeva, V. S. Slyshenkov, M. R. Wieçkowski, and L. Wojtczak.** Photomodification of mitochondrial proteins by azido fatty acids and its effect on mitochondrial energetics. A further evidence for the role of the ADP/ATP carrier in fatty acid-mediated uncoupling. *Eur. J. Biochem.* 240: 387–393, 1996.
31. **Skulachev, V. P.** Fatty acid circuit as a physiological mechanism of uncoupling of oxidative phosphorylation. *FEBS Lett.* 294: 158–162, 1991.

Exhibit F

1: Biotechniques. 1991 Sep;11(3):313-4, 316-8.

Links

DNA transfection in COS cells: a low-cost serum-free method compared to lipofection.

Lévesque JP, **Sansilvestri P**, **Hatzfeld A**, **Hatzfeld J**.

Laboratoire C.N.R.S., I.C.I.G. Hôpital Paul-Brousse, Villejuif, France.

We describe a defined medium that allows efficient DNA transfections in COS cells and transient expression of the corresponding recombinant protein in serum-free conditions. With a modified DEAE-dextran/chloroquine method, we obtained 80% more transfected cells expressing the recombinant human interleukin-2 receptor than with transfection with cationic liposomes, one of the most efficient techniques to date. The absence of serum in the culture medium should reduce subsequent purification steps for production of recombinant mammalian proteins. Moreover, it should allow investigations dealing with the role of serum or other exogenous factors on mRNA stability or post-translation events during protein synthesis.

PMID: 1931028 [PubMed - indexed for MEDLINE]

Exhibit G

paper on methodology

Expression and characterization of recombinant human lecithin:cholesterol acyltransferase

John S. Hill, Karmin O, Xingbo Wang, S. Paranjape,* D. Dimitrijevich,* Andras G. Lacko,* and P. Haydn Pritchard[1]

University Hospital Lipid Research Group, Department of Pathology, University of British Columbia, Vancouver, B.C., Canada, and Department of Biochemistry and Molecular Biology, Texas College of Osteopathic Medicine,* University of North Texas, Fort Worth, TX

Abstract We have established a baby hamster kidney (BHK) cell line that constitutively expresses significant quantities of human recombinant lecithin:cholesterol acyltransferase (rLCAT). LCAT cDNA was cloned into a mammalian expression vector containing the metallothionein promoter and the dihydrofolate reductase gene. After transfection, the BHK cells were treated with 500 μM methotrexate for 2 weeks to select the successfully transfected cells. Surviving colonies were subcloned and high level secretors were identified by measurement of LCAT activity and mass in the culture medium. The attachment of transfected cells to microcarrier beads enabled the efficient production of large quantities of rLCAT in a serum-free medium. After a single-step chromatography procedure, the rLCAT was purified to homogeneity with yields exceeding 1 mg of rLCAT per 100 ml of culture medium. The molecular weight of rLCAT (≈ 66,000) was identical to that of purified human plasma LCAT on SDS polyacrylamide electrophoresis. The rLCAT was activated by apolipoprotein A-I and had an average specific activity that was similar to purified plasma LCAT. After selective deglycosylation with either neuraminidase or N-glycanase, rLCAT and plasma LCAT had identical molecular weights. The simplification of the production and purification of rLCAT reported here will enable a more in depth analysis of the structure and function of this enzyme.—**Hill, J. S., K. O, X. Wang, S. Paranjape, D. Dimitrijevich, A. G. Lacko, and P. H. Pritchard.** Expression and characterization of recombinant human lecithin:cholesterol acyltransferase. *J. Lipid Res.*, 1993. **34:** 1245–1251.

Supplementary key words DNA transfection • expression • recombinant protein • enzymatic deglycosylation

Lecithin:cholesterol acyltransferase (LCAT; EC 2.3.1.43) catalyzes the transfer of an acyl group from the *sn*-2 position of phosphatidylcholine to the 3-hydroxyl group of cholesterol, resulting in the formation of cholesteryl ester and lysophosphatidylcholine. LCAT is synthesized in the liver and secreted into plasma where it associates with high density lipoproteins (HDL) (1, 2). These spherical and nascent discoidal particles contain apolipoprotein A-I which is necessary for maximum LCAT activity (3). By catalyzing the production of the majority of cholesteryl esters in human plasma, LCAT creates an unesterified cholesterol gradient between plasma membranes and circulating lipoproteins, thus facilitating the transport of cholesterol from peripheral tissues to the liver.

The mature LCAT protein is a single polypeptide of 416 amino acids with a relative molecular mass of 65,000–69,000 (4) containing 24% carbohydrate of which up to 7% is sialic acid (5). The primary structure of human LCAT has been determined by the cloning and sequencing of LCAT cDNA (6) and by direct amino acid sequencing (7). The analysis of specific chemical modifications of purified human plasma LCAT (8–10) has provided some insight into the topology of the active site of LCAT. More recently, the catalytic mechanism has been investigated by site-directed mutagenesis (11, 12). Studies with inhibitors of N-linked glycosylation (13) in Chinese hamster ovary (CHO) cells secreting recombinant human LCAT (rLCAT) have also been performed. An in depth analysis of the structure and function of LCAT has often been limited by either the labor-intensive procedures required for the purification of the plasma enzyme or the inability to produce large quantities of rLCAT from cell culture.

To further these investigations, we have developed a baby hamster kidney (BHK) cell line that constitutively expresses significant quantities of rLCAT. In addition, we describe the efficient production and purification of rLCAT including comparative data characterizing both plasma and rLCAT enzyme species.

Abbreviations: rLCAT, (recombinant) lecithin:cholesterol acyltransferase; HDL, high density lipoprotein; apoA-I, apolipoprotein A-I; CHO, Chinese hamster ovary; BHK, baby hamster kidney; DMDM, Dulbecco's modified Eagle's medium; FBS, fetal bovine serum; TBS, Tris-buffered saline; HBS, HEPES-buffered saline.

[1]To whom correspondence should be addressed at: Department of Pathology, The Research Center, 950 West 28th Avenue, Vancouver, B.C., Canada V5Z 4H4.

MATERIALS AND METHODS

Plasmid construction and DNA transfection

Full length LCAT cDNA (6) contained within pUC19 was kindly supplied by John McLean, Genentech Inc., San Francisco. The LCAT cDNA was released from this vector by digesting with EcoRI and BamHI. After purification by agarose electrophoresis, the LCAT cDNA fragment was blunt-ended with Klenow polymerase and subsequently ligated into the SmaI restriction site of the pNUT expression vector (14, 15). The newly formed pNUTLCAT plasmid, which places the LCAT cDNA under the control of the mouse metallothionein promoter, was used to establish stable cell lines of baby hamster kidney (BHK) cells, which constitutively synthesize the native LCAT protein. In addition, the pNUT vector contains a mutant form of the dihydrofolate reductase (DHFR) gene permitting the selection of cells stably transfected with the plasmid DNA by their survival in high concentrations of methotrexate.

BHK cells were maintained in Dulbecco's modified Eagle's medium (DMEM;Gibco-BRL) supplemented with 10% heat-inactivated fetal bovine serum (FBS). To mediate the transfection of BHK cells, coprecipitates of plasmid DNA (pNUT or pNUTLCAT) and $CaPO_4$ were prepared (16). Plasmid DNA (20–30 μg) in 0.50 ml of 0.25 M $CaCl_2$ was mixed with 2× HEPES-buffered saline (2× HBS) containing 40 mM HBS (pH 6.96), 280 nM NaCl, 10 mM KCl, 1.5 mM Na_2HPO_4, and 10 mM glucose. The calcium phosphate–DNA mixture was incubated at room temperature for 30 min before it was added dropwise to a 100-mm culture dish containing a 50% confluent BHK monolayer. After an overnight incubation at 37°C under 5% CO_2, the transfection medium was replaced with DMEM/10% FBS for 24 h before transfected cells were selected over a period of 10–14 days in DMEM/10% FBS containing 500 μM methotrexate (15). Surviving colonies were transferred to 20-mm culture wells and grown to confluency under selected conditions. Clones expressing maximal quantities of LCAT were identified by LCAT enzyme activity and solid-phase LCAT immunoassay. One cell line, termed BHK-LCAT1, was selected for further analysis.

Endogenous radiolabeling and immunoadsorption of rLCAT

BHK-LCAT1 cells were incubated in methionine-free DMEM (DMEM-Met) for 20 min at 37°C to deplete the methionine pool. The endogenous methionine pool was then labeled for 30 min in DMEM-Met supplemented with 100–200 μCi/ml [^{35}]methionine (700 Ci/mmol, New England Nuclear). Subsequently, the labeling medium was removed and the cells were incubated with DMEM/10% FBS. After a specified incubation period, the medium was collected and the cellular protein was harvested in lysis buffer (50 mM Tris-HCl, pH 8.0, 62.5 mM EDTA, 1% Nonidet P40, 0.4% sodium deoxycholate, and 1 mM phenylmethylsulfonylfluoride) for subsequent analysis.

Solid phase immunoadsorption was used to detect the presence of LCAT in the culture medium as described previously (17). Polyclonal goat anti-human LCAT antibodies were pre-adsorbed onto agarose-immobilized protein G (GammaBind G Sepharose, Pharmacia LKB) for 30 min at 4°C. Subsequently, a sample volume of medium was added to the suspension and the mixture was rotated end-over-end overnight at 4°C. After centrifugation and washing, the adsorbed material was then eluted from the agarose beads by heating at 90°C in the presence of 2× sodium dodecyl sulfate (SDS) sample buffer (0.1 M Tris-HCl, pH 6.8, 2% SDS, 40% glycerol). The beads were removed by centrifugation and the supernatant was recovered for electrophoretic analysis. [^{14}C]methylated protein molecular weight markers (Amersham Canada Ltd., Oakville, Ontario) were used as standards. Before autoradiography, the fixed gels were equilibrated with Amplify (Amersham Canada Ltd.) and dried onto Whatman 3MM chromatography paper. Autoradiograms were exposed on X-Omat AR film (Eastman-Kodak) for 16–24 h.

Culture conditions for the optimal secretion of rLCAT by BHK-LCAT1 cells

To maximize the surface area available for cell growth, porous microcarrier beads (Cultisphere-G, Hyclone Laboratories, Inc. Logan Utah) were used. BHK-LCAT1 cells (2 × 10^8) and 350 mg of sterile microcarrier beads were suspended in DMEM for 24 h permitting the attachment of cells to the beads. Subsequently, the cells were incubated in DMEM/10% FBS while the culture suspension was stirred at a rate of 15 rev/min for 1 minute every hour. After a 4-day growth period, the medium was changed to serum-free Opti-MEM (Gibco-BRL). After 72 h of incubation the culture medium was collected for purification.

Purification of rLCAT

Approximately 300 ml of culture medium containing rLCAT was loaded onto a phenyl-Sepharose column (10 × 15 cm) that was previously equilibrated with 0.005 M sodium phosphate, 0.3 M sodium chloride, pH 7.4. The column was washed with the same buffer until the absorbance (280 nm) fell below 0.01. Subsequently, the rLCAT was eluted with deionized water.

Antibody preparation

Human plasma LCAT was purified to homogeneity using a modification of a previously described method (18). The dodecylamine-agarose and HDL agarose columns were replaced with three columns connected in sequence: phenyl-Sepharose, Affigel-Blue, and heparin-Sepharose.

The final purified LCAT fraction was used to immunize a goat.

LCAT mass assay

The immunoassay of LCAT was carried out as described previously (17) by using nitrocellulose membranes as a solid phase support. Samples containing either culture medium or purified recombinant LCAT standard were bound to the membrane in a Bio-Rad slot-blot apparatus. Polyclonal goat anti-human LCAT antibodies and Protein G conjugated to horseradish peroxidase (Protein G-HRP, Bio-Rad) were used to visualize the protein. The blot was scanned using a Bio-Rad Video Densitometer (Model 620). Total protein determinations were carried out according to Markwell et al. (19) using bovine serum albumin as the standard.

Electrophoresis and immunoblotting

Samples containing LCAT were mixed 1:1 with 2× SDS sample buffer containing 10% β-mercaptoethanol and 0.1% bromphenol blue. The mixture was boiled for 5 min prior to loading onto a 10% polyacrylamide gel run at a constant current of 15 mA/gel for 45 min. Gels were electroblotted onto nitrocellulose paper (0.45 μM) as described by Towbin, Staehelin, and Gordon (20). Membranes were incubated with polyclonal goat anti-human LCAT antibodies and Protein G-HRP as described earlier to detect the LCAT protein.

LCAT activity assay

LCAT activity was measured using single bilayer vesicles prepared by the method of Batzri and Korn (21). Each assay contained 4.66 nmol of unesterified [^{3}H]cholesterol and 10 μg of apolipoprotein A-I. The molar ratio of cholesterol to egg yolk phosphatidylcholine was 1:4. The substrate (0.03 ml) was pre-incubated with apolipoprotein A-I (apoA-I) in 0.15 ml of 0.1 M Tris and 0.15 M NaCl at 37°C for 30 min. Esterification rates were measured over a period of 30 min at 37°C using 0.015 ml of plasma or culture medium containing rLCAT. The reaction was stopped by adding chloroform–methanol 2:1 and incubating for 2 h at room temperature to extract lipids. Labeled cholesterol and cholesteryl ester were separated by thin-layer chromatography on silica gel layers incubated in petroleum ether–diethyl ether–acetic acid 70:12:1 and radioactivity was determined by liquid scintillation spectrometry.

LCAT activities based on the method of Manabe et al. (22) measured during the production of rLCAT were carried out using the exogenous substrate containing apoA-I.

Enzymatic deglycosylation of LCAT

Neuraminidase (*Clostridium perfringens*, type V, Sigma Chemical Co.) was used to remove the sialic acid residues from LCAT by adding 3 μl of neuraminidase (1 U/ml) to 7 μl of culture medium or purified human LCAT. Samples were incubated at 37°C for 1 h. N-glycanase digestion was performed by adding 10 μl of 0.9 M sodium phosphate, pH 8.7, and 4 μl of 10% Nonidet P-40 to 15 μl of sample. The mixture was boiled for 10 min, cooled, and 1 μl of N-glycanase (250 U/ml) was added before incubating at 37°C overnight. Endoglycosidase H digestion was carried out by adding 10 μl of 0.15 M sodium acetate buffer, pH 5.8, and 4 μl of 10% Nonidet P-40 to 15 μl of sample. The mixture was boiled for 10 min, cooled, and 2 μl of endoglycosidase H (1 U/ml) was added before incubating at 37°C for 16 h.

RESULTS

Expression of rLCAT in BHK cells

The autoradiogram in **Fig. 1** indicates that BHK cells transfected with pNUTLCAT secreted a predominant protein that was recognized by antibodies specific for human plasma LCAT. This protein migrated as a broad band typical of glycosylated proteins in SDS-polyacrylamide gels and spanned a molecular weight of 60,000–67,000. This is consistent with previous determinations for purified human LCAT (4, 5). No LCAT mass was detected in the medium from those cells transfected with the pNUT vector containing no LCAT cDNA insert.

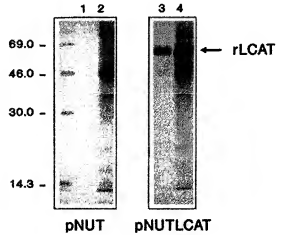

Fig. 1. Expression of rLCAT. BHK cells transfected with pNUT or pNUTLCAT plasmids were subsequently labeled with [^{35}S]methionine for a 30-min pulse. After 6 h (lanes 1 and 3) and 24 h (lanes 2 and 4) of incubation, medium was collected and rLCAT was immunoadsorbed as described in Materials and Methods. The immunoadsorbed protein was reduced and electrophoresed in 10% SDS-polyacrylamide gels. After gel drying, radioactivity was detected by autoradiography. Lanes 3 and 4 show labelled rLCAT (60,000–67,000) secreted by BHK cells transfected with pNUTLCAT. Lanes 1 and 2 represent cells transfected with the pNUT vector containing no LCAT CDNA insert. Molecular weight standards are indicated in kilodaltons.

JOURNAL OF LIPID RESEARCH ASBMB

Properties of rLCAT

Aliquots of serum-free medium were collected at several time intervals from 35-mm culture dishes containing BHK-LCAT1 cells and assayed for the presence of LCAT mass and activity. As shown in **Table 1,** the levels of both LCAT mass and activity continued to increase during a 48-h incubation period. The average specific activity of the LCAT enzyme calculated from these values of mass and activity was 3.75 ± 0.39 nmol/h per μg. The specific activity of rLCAT was similar to plasma LCAT (5.64 ± 0.32 nmol/h per μg) (23) and LCAT purified from plasma (0.75± 0.08 nmol/h per μg) using the same substrate. In addition, the ability of apoA-I to activate both rLCAT and human plasma LCAT was compared. Both enzymes demonstrated a typical saturation curve with a maximal activation between 5 and 7.5 μg of apoA-I/assay (**Fig. 2**). After numerous cell passages, both the activity and mass of rLCAT secreted from this stable BHK cell line remained consistent.

Production and purification of rLCAT

As mentioned previously, the LCAT cDNA is under the control of the mouse metallothionein promoter which can be stimulated by the presence of divalent cations (24). Due to its lower cell toxicity, the effect of Zn^{2+} ion concentration on the secretion of rLCAT from the BHK-LCAT1 cells was investigated. As shown in **Fig. 3,** a Zn^{2+} ion concentration of 20 μM corresponded to the highest secretion rate of rLCAT.

After a 72-h incubation in serum-free Opti-MEM, BHK cells attached to microcarrier beads secreted rLCAT at levels exceeding 10 μg/ml. The secreted rLCAT was purified by phenyl-Sepharose chromatography with the elution profile depicted in **Fig. 4.** After elution with deionized water, 97% of the original activity was recovered resulting in a 29-fold purification (**Table 2**). A homogeneous LCAT protein was eluted from the column as observed by a single band in SDS polyacrylamide electrophoresis.

TABLE 1. Secretion of rLCAT mass and activity into serum-free medium

Hours of Incubation	Mass	Activity	Specific activity
	μg/ml	*nmol/h/ml*	*nmol/h/μg*
24	4.36	17.90	4.11
30	6.91	26.39	3.82
48	10.30	34.30	3.33

Confluent BHK-LCAT1 cells were incubated in serum-free Opti-MEM for the indicated time intervals. LCAT activity and mass were determined as described in Materials and Methods. Activity units are expressed as nmol of cholesteryl ester formed per hour per ml. The values depicted are the mean of two separate experiments, each done in duplicate.

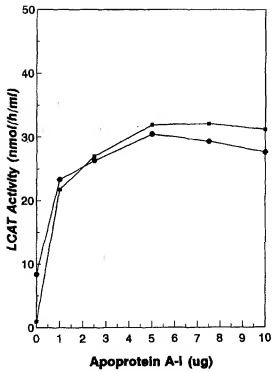

Fig. 2. Activation of plasma LCAT and rLCAT as a function of apolipoprotein A-I concentration. Assays were performed by using single bilayer cholesterol–lecithin 1:4 vesicles. LCAT activity was measured using 0.015 ml of plasma (●) or culture medium containing rLCAT (■) and expressed as nmol of cholesteryl ester formed per hour per ml. Data points are means of duplicate assays.

Enzymatic deglycosylation of plasma LCAT and rLCAT

To compare the carbohydrate structure of purified human LCAT and rLCAT, each was selectively deglycosylated with either neuraminidase to remove sialic acid residues or N-glycanase to digest N-linked carbohydrate chains. **Fig. 5** shows a Western blot of an SDS polyacrylamide gel which demonstrates that both enzymes have equivalent molecular weights before and after enzymatic deglycosylation. However, it is apparent that rLCAT migrates as a broader band compared to plasma LCAT. Digestion with neuraminidase was accompanied by a reduction in molecular weight which was consistent with previous data (5, 12) indicating that sialic acid makes up a significant portion of the total carbohydrate mass. In addition, reaction with N-glycanase reduced the apparent molecular weight of LCAT to about 48,000, which was comparable to the calculated molecular weight for the mature protein of 47,090 (6). In addition, the removal of the N-linked carbohydrate significantly decreased the size heterogeneity of rLCAT. Both plasma LCAT and rLCAT were resistant to digestion with endoglycosidase H (data not shown) in-

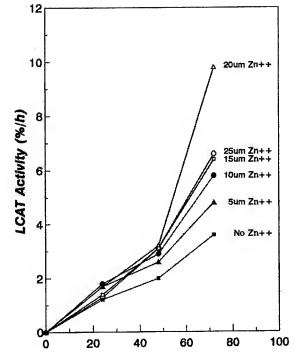

Fig. 3. Effect of Zn^{2+} ion concentration on the secretion of rLCAT. Different concentrations of $ZnSO_4$ were added to a suspended culture of BHK-LCAT1 cells after the initiation of incubation in serum-free medium. Culture medium was analyzed for LCAT activity expressed as a percentage of cholesterol esterified per hour.

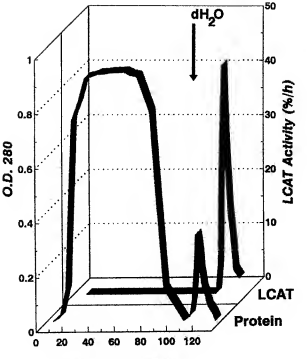

Fig. 4. Elution profile of phenyl-Sepharose CL-4B chromatography. An aliquot (300 ml) of culture medium containing rLCAT secreted from BHK cells was applied to a phenyl-Sepharose CL-4B column (10 × 15 cm) equilibrated with 0.005 M potassium phosphate buffer (pH 7.4) containing 0.5 M sodium chloride. The column was washed with the same buffer until the absorbance (280 nm) fell below 0.01 at which point the rLCAT was eluted with deionized water (arrow). The protein absorbance and LCAT activity expressed as a percentage of cholesterol esterified per hour were determined in each fraction.

dicating the assembly of either complex or hybrid oligosaccharide chains in the Golgi apparatus prior to the secretion of LCAT from the cell (25).

DISCUSSION

In this study, we have stably transfected BHK cells with an expression vector containing an LCAT cDNA. The cells secrete rLCAT whose properties closely resemble those of plasma LCAT with respect to molecular weight, activation by apoA-I, specific activity, and carbohydrate content. However, there was a greater size heterogeneity associated with rLCAT in SDS polyacrylamide electrophoresis when compared to LCAT purified from plasma. Similar observations have recently been reported for recombinant antithrombin secreted from BHK and CHO cells (26). In each case, removal of the N-linked carbohydrate resulted in the migration of a single sharp band with no apparent difference in mobility compared to the plasma protein, suggesting a greater degree of heterogeneity in the glycosylation of the recombinant protein. To determine the basis for these differences, a comparative analysis of the specific composition and structure of the carbohydrate chains for both rLCAT and plasma LCAT is currently under investigation. It is possible that

TABLE 2. Purification of rLCAT secreted by transfected BHK cells

Fraction	Volume	Protein	Specific Activity	Purification	Yield
	ml	*mg*	*units/mg*	*-fold*	%
Opti-MEM culture medium	350	149	105		100
Phenyl-Sepharose eluent	110	4.9	3,090	29	97

Fig. 5. Comparison of the effects of enzymatic deglycosylation of human and rLCAT. The molecular weights of human plasma LCAT and rLCAT were determined by SDS polyacrylamide gel electrophoresis. LCAT protein was blotted onto nitrocellulose membranes and detected immunologically as described in Materials and Methods. Lane 1, untreated rLCAT; lane 2, untreated human plasma LCAT; lane 3, neuraminidase-treated rLCAT; lane 4, neuraminidase-treated human plasma LCAT; lane 5, N-glycanase-treated rLCAT; lane 6, N-glycanase-treated human LCAT.

differences in the specific activity of LCAT reported for different cell lines such as COS-1 cells, 3–12 nmol/h per μg (17, 27); CHO cells, 1–2 nmol/h per μg (11–13); and human embryonic-293 cells, 46 nmol/h per μg (28) could be attributed in part to differences in the glycosylation patterns present in each mammalian cell type. In addition, the variety of methods employed for substrate preparation and activity analysis are also likely to contribute to this heterogeneity.

The increased surface area of microcarrier beads permitted a greater number of cells to grow per unit volume of culture medium. This form of tissue culture in conjunction with the use of serum-free medium has enabled us to produce greater quantities of rLCAT which can be purified to homogeneity by a single-step chromatography procedure.

The simplification of the production and purification of rLCAT reported here will pave the way for a more in depth analysis of the structure and function of this enzyme. The knowledge of natural mutations causing fish eye disease (23, 29, 30) and LCAT deficiency (26, 27, 31–33) combined with the application of site-directed mutagenesis will enable the expression and purification of mutant recombinant proteins. As a result, this expression system will be an invaluable tool to investigate the physical/chemical properties of these mutant LCAT proteins and their interaction with lipoproteins. Finally, the preparation of large quantities of homogeneous enzyme should allow the crystallization of LCAT and the elucidation of its three-dimensional structure.

This work was supported by grants from the Medical Research Council of Canada, BC Heart Foundation, and BC Health Care Research Foundation. We would like to acknowledge the help and support of Roger McLeod, Lida Adler, and Jiri Frohlich. In addition, we thank Ross MacGillivray for supplying us with the pNUT expression vector used in these studies.

Manuscript received 28 September 1992 and in revised form 1 March 1993.

REFERENCES

1. Marcel, Y. L., C. Vezina, D. Edmond, and G. Suzue. 1980. Heterogeneity of human high density lipoprotein: presence of lipoproteins with and without apoE and their roles as substrates for lecithin:cholesterol acyltransferase reaction. *Proc. Natl. Acad. Sci. USA.* **177:** 2969–2973.
2. Glomset, J. A. 1972. Plasma lecithin:cholesterol acyltransferase. *In* Blood Lipids and Lipoproteins: Quantitation, Composition and Metabolism. G. J. Nelson, editor. John Wiley & Sons, New York. 745–787.
3. Fielding, C. J., V. G. Shore, and P. E. Fielding. 1972. A protein cofactor of lecithin:cholesterol acyltransferase. *Biochem. Biophys. Res. Commun.* **46:** 1493–1498.
4. Marcel, Y. L. 1982. Lecithin:cholesterol acyltransferase and intravascular transport. *Adv. Lipid Res.* **19:** 85–136.
5. Chung, J., D. A. Abano, G. M. Fless, and A. M. Scanu. 1979. Isolation, properties, and mechanism of in vitro action of lecithin:cholesterol acyltransferase from human plasma. *J. Biol. Chem.* **254:** 7456–7464.
6. McLean, J., C. Fielding, D. Drayna, H. Dieplinger, B. Baer, W. Kohr, W. Henzel, and R. Lawn. 1986. Cloning and expression of human lecithin:cholesterol acyltransferase cDNA. *Proc. Natl. Acad. Sci. USA.* **83:** 2335–2339.
7. Yang, C., D. Manoogian, Q. Pao, F. Lee, R. D. Knapp, A. M. Gotto, Jr., and H. J. Pownall. 1987. Lecithin:cholesterol acyltransferase. *J. Biol. Chem.* **262:** 3086–3091.
8. Jauhiainen, M., and P. J. Dolphin. 1986. Human plasma lecithin:cholesterol acyltransferase: an elucidation of the catalytic mechanism. *J. Biol. Chem.* **261:** 7032–7043.
9. Jauhiainen, M., K. J. Stevenson, and P. J. Dolphin. 1988. Human plasma lecithin:cholesterol acyltransferase: the vicinal nature of the cysteine 31 and cysteine 184 in the catalytic site. *J. Biol. Chem.* **263:** 6526–6533.
10. Jauhiainen, M., W. Yuan, M. H. Gelb, and P. J. Dolphin. 1989. Human plasma lecithin:cholesterol acyltransferase: inhibition of the phospholipase A2-like activity by *sn*-2-difluoroketone phosphatidylcholine analogues. *J. Biol. Chem.* **264:** 1963–1967.
11. Francone, O. L., and C. J. Fielding. 1991. Effects of site-directed mutagenesis at residues cysteine-31 and cysteine-184 on lecithin:cholesterol acyltransferase activity. *Proc. Natl. Acad. Sci. USA.* **88:** 1716–1720.
12. Francone, O. L., and C. J. Fielding. 1991. Structure–function relationships in human lecithin:cholesterol acyltransferase. Site-directed mutagenesis at serine residues 181 and 216. *Biochemistry.* **30:** 10074–10077.
13. Collet, X., and C. J. Fielding. 1991. Effects of Inhibitors of N-linked oligosaccharide processing on the secretion, stability, and activity of lecithin:cholesterol acyltransferase. *Biochemistry.* **30:** 3228–3234.
14. Palmiter, R. D., R. R. Behringer, C. J. Quaife, F. Maxwell, I. H. Maxwell, and R. L. Brinster. 1987. Cell lineage ablation in transgenic mice by cell-specific expression of a toxin gene. *Cell.* **50:** 435–443.
15. Funk, W. D., R. T. A. MacGillivray, A. B. Mason, S. A. Brown, and R. C. Woodworth. 1990. Expression of the amino-terminal half-molecule of human serum transferrin in cultured cells and characterization of the recombinant protein. *Biochemistry.* **29:** 1654–1660.
16. Chen, C., and H. Okayama. 1987. High-efficiency transformation of mammalian cells by plasmid DNA. *Mol. Cell Biol.* **7:** 2745–2752.
17. O, K., J. S. Hill, X. Wang, and P. H. Pritchard. 1993. Recombinant lecithin:cholesterol acyltransferase containing a $Thr_{123} \rightarrow Ile$ mutation esterifies cholesterol in low den-

sity lipoprotein but not in high density lipoprotein. *J. Lipid Res.* **34:** 81–88.
18. Park, Y. B., and A. G. Lacko. 1986. Isolation and characterization of lecithin:cholesterol acyltransferase from hog plasma. *Biochim. Biophys. Acta.* **877:** 179–190.
19. Markwell, M. K., S. M. Haas, L. L. Bieber, and N. E. Tolbert. 1978. A modification of the Lowry procedure to simplify protein determination in membrane and lipoprotein samples. *Anal. Biochem.* **87:** 206–210.
20. Towbin, H., T. Staehelin, and J. Gordon. 1979. Electrophoretic transfer of proteins from polyacrylamide gels to nitrocellulose sheets: procedure and some applications. *Proc. Natl. Acad. Sci. USA.* **76:** 4350–4354.
21. Batzri, S., and E. D. Korn. 1973. Single-layer liposomes prepared without sonication. *Biochim. Biophys. Acta.* **298:** 1015–1019.
22. Manabe, M., T. Abe, M. Nozawa, A. Maki, M. Hirata, and H. Itakura. 1987. New substrate for determination of serum lecithin:cholesterol acyltransferase. *J. Lipid Res.* **28:** 1206–1215.
23. Funke, H., A. von Eckardstein, P. H. Pritchard, J. J. Albers, J. J. P. Kastelein, C. Droste, and G. Assmann. 1991. A molecular defect causing fish eye disease: an amino acid exchange in lecithin:cholesterol acyltransferase (LCAT) leads to the selective loss of α-LCAT activity. *Proc. Natl. Acad. Sci. USA.* **88:** 4855–4859.
24. Stuart, G. W., P. F. Searle, H. Y. Chen, R. L. Brinster, and R. D. Palmiter. 1984. A 12-base-pair DNA motif that is repeated several times in metallothionein gene promoter confers metal regulation to a heterologous gene. *Proc. Natl. Acad. Sci. USA.* **81:** 7318–7322.
25. Tarentino, A. L., T. H. Plummer, and F. Maley, 1974. The release of intact oligosaccharides from specific glycoproteins by endo-β-N-acetylglucosaminidase H. *J. Biol. Chem.* **249:** 818–824.
26. Bjork, I., K. Ylinenjarvi, S. T. Olson, P. Hermentin, H. S. Conradt, and G. Zettlmeissl. 1992. Decreased affinity of recombinant antithrombin for heparin due to increased glycosylation. *Biochem. J.* **286:** 793–800.
27 Taramelli, R., M. Pontoglio, G. Candiani, S. Ottolenghi, H. Dieplinger, A. Catapano, J. Albers, C. Vergani, and J. McLean. 1990. Lecithin:cholesterol acyltransferase deficiency: molecular analysis of a mutated allele. *Hum. Genet.* **85:** 195–199.
28. Klein, H-G., P. Lohse, N. Duverger, J. J. Albers, D. J. Rader, L. A. Zech, S. Santamarina-Fojo, and H. B. Brewer, Jr. 1993. Two different allelic mutations in the lecithin:cholesterol acyltransferase (LCAT) gene resulting in classic LCAT deficiency: LCAT ($tyr^{83} \rightarrow$stop) and LCAT ($tyr^{156} \rightarrow$asn). *J. Lipid Res.* **34:** 49–58.
29. Klein, H-G., P. Lohse, P. H. Pritchard, D. Bojanovski, H. Schmidt, and H. B. Brewer, Jr. 1992. Two different allelic mutations in the lecithin:cholesterol acyltransferase gene associated with the fish eye syndrome. *J. Clin. Invest.* **89:** 499–506.
30. Skrettingˊ, G., and H. Prydz. 1992. An amino acid exchange in exon I of the human lecithin:cholesterol acyltransferase (LCAT) gene is associated with fish eye disease. *Biochem. Biophys. Res. Commun.* **182:** 583–587.
31. Gotoda, T., N. Yamada, T. Murase, M. Sakuma, N. Murayama, H. Shimano, K. Kozaki, J. J. Albers, Y. Yazaki, and Y. Akanuma. 1991. Differential phenotypic expression by three mutant alleles in familial lecithin:cholesterol acyltransferase deficiency. *Lancet.* **338:** 778–781.
32. Bujo, H., J. Kusunoki, M. Ogasawara, T. Yamamoto, Y. Ohta, T. Shimada, Y. Saito, and S. Yoshida. 1991. Molecular defect in familial lecithin:cholesterol acyltransferase (LCAT) deficiency: a single nucleotide insertion in LCAT gene causes a complete deficient type of the disease. *Biochem. Biophys. Res. Commun.* **181:** 933–940.
33. Skrettingˊ, G., J. P. Blomhoff, J. Solheim, and H. Prydz. 1991. The genetic defect of the original Norwegian lecithin:cholesterol acyltransferase deficiency families. *FEBS Lett.* **309:** 307–310.

Exhibit H

1: Cytotechnology. 1990 Jul;4(1):39-43.

Links

Expression of human lymphotoxin in Namalwa KJM-1 cells adapted to serum-free medium.

Miyaji H, Harada N, Mizukami T, Sato S, Fujiyoshi N, Itoh S.

Tokyo Research Laboratories, Kyowa Hakko Kogyo Co., Ltd., Japan.

A Namalwa cell line, KJM-1, which was adapted to serum-free medium is thought to be a good host cell line for recombinant DNA technology. We previously reported the expression of human beta-interferon (beta-IFN) in Namalwa KJM-1 (Miyaji, 1989a). The utility of Namalwa KJM-1 for expression of foreign genes was further examined. As a target gene to be expressed, human lymphotoxin (hLT) cDNA was used. It was engineered for expression in Namalwa KJM-1 using a simian virus 40 (SV40)-based expression vector pAGE107 (Miyaji, 1989a). It contains all components necessary for the expression of cDNA in mammalian cells. The expression vector was introduced into Namalwa KJM-1 by electroporation. Among the transformants, clone 7 was further examined for the expression of hLT in serum-free medium. The production level of hLT was augmented with the increase of the cell density. Thus it was further indicated that Namalwa KJM-1 is useful for production of foreign gene products.

PMID: 1369278 [PubMed - indexed for MEDLINE]

Exhibit I

THE JOURNAL OF BIOLOGICAL CHEMISTRY
Vol. 270, No. 23, Issue of June 9, pp. 14220–14228, 1995
Printed in U.S.A.

Production of Human Secretory Component with Dimeric IgA Binding Capacity Using Viral Expression Systems*

(Received for publication, March 2, 1995, and in revised form, April 10, 1995)

Lorenz Rindisbacher‡, Sandra Cottet‡, Riccardo Wittek‡, Jean-Pierre Kraehenbuhl§, and Blaise Corthésy‡¶

From the ‡Institut de Biologie Animale, Bâtiment de Biologie, Université de Lausanne, CH-1015 Lausanne, Switzerland and the §Swiss Institute for Experimental Cancer Research and Institute of Biochemistry, University of Lausanne, CH-1066 Epalinges, Switzerland

The cDNA encoding the NH_2-terminal 589 amino acids of the extracellular domain of the human polymeric immunoglobulin receptor was inserted into transfer vectors to generate recombinant baculo- and vaccinia viruses. Following infection of insect and mammalian cells, respectively, the resulting truncated protein corresponding to human secretory component (hSC) was secreted with high efficiency into serum-free culture medium. The Sf9 insect cell/baculovirus system yielded as much as 50 mg of hSC/liter of culture, while the mammalian cells/vaccinia virus system produced up to 10 mg of protein/liter. The M_r of recombinant hSC varied depending on the cell line in which it was expressed (70,000 in Sf9 cells and 85–95,000 in CV-1, TK− 143B and HeLa). These variations in M_r resulted from different glycosylation patterns, as evidenced by endoglycosidase digestion. Efficient single-step purification of the recombinant protein was achieved either by concanavalin A affinity chromatography or by Ni^{2+}-chelate affinity chromatography, when a 6xHis tag was engineered to the carboxyl terminus of hSC. Recombinant hSC retained the capacity to specifically reassociate with dimeric IgA purified from hybridoma cells.

Mucosal epithelia of the human body, including the linings of the digestive, respiratory, and urogenital systems, comprise a vast surface permanently vulnerable to attack by outside pathogens. Protection of mucosal surfaces against colonization and possible invasion by pathogenic microorganisms is mediated by a special class of antibodies known as secretory immunoglobulin A (sIgA)[1] (Mestecky and McGhee, 1987; Brandtzaeg, 1989; Kraehenbuhl and Neutra, 1992a). The antibodies are believed to act by agglutinating potential invaders and facilitate their clearance by peristaltic or mucociliary movement.

The IgA moiety is produced by local mucosal and glandular plasma cells. Two immunoglobulin A (IgA) antibodies are dimerized via J chain in a tail to tail arrangement; the addition of J chain occurs in plasma cells just before secretion (Parkhouse and Della Corte, 1973; McCune et *al.*, 1981). To interact with pathogens on the luminal side of the mucosa, the dimeric IgA (dIgA) antibodies have to be transported across the epithelium barrier by the poly-immunoglobulin receptor (pIgR). The receptor, a type I transmembrane protein, is expressed by the epithelial cells on the basolateral side of the epithelia lining mucosal and glandular surfaces. Upon binding to the receptor, the receptor-ligand complex is internalized and transcytosed (Schaerer et *al.*, 1991); during transport or at the apical cell surface, the pIgR is cleaved and the extracellular portion of the molecule, termed secretory component (SC), is released free or bound to IgA (for review, see Mestecky *et al.* (1991), Kraehenbuhl and Neutra (1992b), and Neutra *et al.* (1994)). Studies on the stoichiometry of SC-IgA association suggested that either one or two molecules of SC are contained per sIgA complex (Kühn and Kraehenbuhl, 1982).

The initial binding of SC to dimeric IgA *in vitro* is noncovalent, and interchain disulfide bridges are formed in a second step (Lindh and Björk, 1977; Garcia-Pardo et *al.* 1979; Eiffert et *al.*, 1984). The noncovalent interaction has been shown to be mediated by the amino-terminal domain of rabbit SC (Frutiger et *al.*, 1986) and human SC (Bakos et *al.*, 1991). Binding of SC to IgA confers resistance to proteolytic enzymes, including Pronase, papain, trypsin, and pepsin (Underdown and Dorrington, 1974; Lindh, 1975). Brown et *al.* (1970) have shown that sIgA in duodenal secretions is more resistant than monomeric IgA to the action of proteases. Recently it was reported that human SC was able to compete the binding of *Helicobacter pylori* to a gastric epithelial receptor by virtue of fucosyl residues associated with SC carbohydrate side chains (Falk *et al.*, 1993; Boren *et al.*, 1993).

Despite the discovery of SC almost three decades ago, little is known about the properties the molecule confers to dimeric IgA antibodies, except for resistance to proteolysis. In order to analyze the molecular role of SC on IgA stability and determine its contribution to immune protection, both monoclonal IgA antibodies and the same antibodies reassociated with SC have to be available. Although protocols have been established for the production of monoclonal dimeric IgA antibodies (Lee *et al.*, 1994), their combination to SC has been hampered by the difficulty to produce sufficient amounts of recombinant SC. The aim of this study was therefore to produce milligram quantities of hSC using recombinant virus expression systems and insect or mammalian cells.

We report here that recombinant hSC (*a*) is produced and secreted with high efficiency by both insect and mammalian

* This work was supported by research funds from the Swiss National Science Foundation, Biotechnology Priority Program, Grant 5002-034603 (to L. R., J.-P. K., and B. C.) and from the Etat de Vaud (to S. C. and R. W.). The costs of publication of this article were defrayed in part by the payment of page charges. This article must therefore be hereby marked "*advertisement*" in accordance with 18 U.S.C. Section 1734 solely to indicate this fact.

¶ To whom correspondence should be addressed. Tel.: 41-21-692-41-38; Fax: 41-21-692-41-05.

[1] The abbreviations used are: sIgA, secretory IgA; pIgR, polymeric immunoglobulin receptor; IgA, immunoglobulin A; dIgA, dimeric IgA; hSC, human secretory component; PCR, polynucleotide chain reaction; m.o.i., multiplicity of infection; Endo H, endoglycosidase H; PNGase F, peptide-*N*-glycosidase F; ConA, concanavalin A; ELISA, enzyme-linked immunosorbent assay; PBS, phosphate-buffered saline; PAGE, polyacrylamide gel electrophoresis; TK, thymidine kinase; DORA, dot blot reassociation assay.

cells, (*b*) is glycosylated by both insect and mammalian cells, yet to a different extent, (*c*) is readily isolated from serum-free culture medium by lectin or ion-chelate affinity chromatographies, and (*d*) binds to dimeric IgA, indicating that the molecule is properly folded and retains its biological activity. This is the first report on the production of biologically active recombinant hSC, that can now be used to dissect the properties it confers to dimeric IgA of defined specificity in *in vitro* systems (Hirt *et al.*, 1993) or upon mucosal administration.

EXPERIMENTAL PROCEDURES

Cell Culture Conditions

African green monkey kidney CV-1 cells (ATCC CCL70) were grown in Dulbecco's modified Eagle's medium supplemented with 8% fetal calf serum containing 50 units/ml penicillin and 50 μg/ml streptomycin. The cells were cultivated to confluency in 175-cm^2 flasks to a final concentration of 2×10^7 cells/flask in a 5% CO_2 atmosphere at 37 °C. Human TK$^-$ 143B cells (ATCC CRL 8303) and human HeLa cells (ATCC CCL 2) were grown under the same conditions. Human HeLa S3 cells (ATCC CCL 2.2; *a clonal derivative of the parent HeLa cell line CCL2*) were grown in spinner bottles at 37 °C, in minimal essential medium for suspension culture supplemented with 8% fetal calf serum, to a concentration of 6×10^6 cells/ml.

Spodoptera frugiperda (Sf9) insect cells (ECACC 89070101) were cultured at 28 °C in TC100 medium (Life Technologies, Inc.) containing 10% fetal calf serum or in SF-900 II medium (Life Technologies, Inc.) in the absence of serum. Cells grown as monolayers in T-flasks were passaged at confluency. Cells in suspension were grown as shaker cultures at 125 rpm in Erlenmeyer flasks and were diluted with fresh medium to 5×10^6 cells/ml twice a week.

Engineering of Human Secretory Component Sequences and Cloning into Viral Transfer Vectors

Human pIgR cDNA was obtained from Dr. Charlotte Kaetzel, University of Cleveland, OH. Since Glu^{569} is suggested to represent the authentic carboxyl terminus of human SC (Krajci *et al.*, 1989; corresponding to Glu^{536} according to their numbering), we introduced a stop codon immediately downstream of this position in the recombinant protein. An *EcoRI-BamH*I fragment containing the hSC Kozak (1986) sequence, the hSC ATG initiation codon, the signal sequence for secretion, and the five extracellular Ig-like domains (Mostov *et al.*, 1984), including Asp^{583}, was subcloned into pBluescriptII KS+ (Stratagene). The sequence corresponding to Pro^{564} to Glu^{569}, including a stop codon and an *Xba*I restriction site, was subsequently introduced 3′ to the *Bam*HI site as a double-stranded oligonucleotide,

```
GATCCCAGGCTTTTGCAGATAGT
    GGTCCGAAAACGTCTCATCAGATC
BamHI          STOP XbaI
```

The resulting construct was referred to as pBS-hSC. The same strategy using the oligonucleotides,

AAATG GGCCGCGCGAAATTATT-3′ as "inside" primers and oligonucleotides 5′-CCATCGATG AAGGACAGTTCTTTCCAG-3′ and 5′-GGGGTACCGGTCACCGTTCTGCCCAGGTCC-3′ as "outside" primers. The PCR products were sequenced by the method of Sanger *et al.* (1977). Plasmids pHGS1-hSC and pHGS1-hSC-6xHis were constructed via a four piece ligation including: (*a*) vector pHGS-1 *ClaI/EcoRI*$_{blunt}$; (*b*) the *ClaI/AccI* PCR fragment containing the modified 5′ end of the hSC gene; (*c*) the *AccI/KpnI* fragment from pCB6-hpIgR containing the central portion of the gene; and (*d*) the *KpnI/XbaI*$_{blunt}$ fragment from pBS-hSC or pBS-hSC-6xHis containing the respective 3′ ends.

Cloning of hSC into the baculovirus insertion vector pVL1392 (Invitrogen) was carried out by ligating the *EcoRI/XbaI* fragments containing the modified cDNAs, excised from pBS-hSC or pBS-hSC-6xHis, into the corresponding restriction sites of pVL1392. The resulting constructs were termed pVL1392-hSC and pVL1392-hSC-6xHis, respectively.

Generation of Vaccinia and Baculovirus Recombinants

The hSC cDNA under control of the 11K promoter was incorporated into the genome of wild-type vaccinia virus strain WR (ATCC VR1354) by homologous recombination into the thymidine kinase (TK) gene. Briefly, subconfluent CV-1 cell monolayers were infected with the temperature-sensitive vaccinia virus ts7 (Drillien and Spehner, 1983) and transfected with WR vaccinia virus DNA and the p11K- or pHGS1-hSC constructs according to Bertholet *et al.* (1985). Thymidine kinase-negative recombinant viruses were selected from the progeny virus by two rounds of plaque purification on TK$^-$ 143B cells in the presence of 75 μg/ml bromodeoxyuridine. Recombinant virus plaques were isolated, and positive clones were identified by PCR screening with primers TKL+ (5′-CGGAACGGCACTATGGACGC-3′) and TKR− (5′-GTCCCATCGAGTGCGGCTAC-3′) specifically hybridizing to regions in the left and right portion of the TK gene flanking the insertion site. Recombinant viruses were amplified by infecting TK$^-$ 143B cell monolayers in the presence of 50 μg/ml bromodeoxyuridine, and large stocks were prepared in CV-1 cells without selection. Recombinant viruses were named after the DNA inserted into the TK locus.

The engineered hSC gene was introduced into the polyhedrin gene of *Autographa californica* multiple nuclear polyhedrosis virus (baculovirus), essentially as described by Summers and Smith (1988), with modifications. Briefly, wild-type baculovirus DNA and transfer plasmids containing the hSC DNA under control of the polyhedrin promoter were cotransfected into Sf9 cells using cationic liposomes (Felgner *et al.*, 1987): 1 ml of TC100 medium without serum containing 1 μg of baculovirus DNA prepared as described (Piwnica-Worms, 1990), 10 μg of pVL1392-hSC or pVL1392-hSC-6xHis, and 30 μl of DOTAP transfection reagent (Boehringer Mannheim) were vigorously mixed for 15 s, incubated at room temperature for 15 min, and added to 2×10^6 adherent Sf9 cells in a 60-mm plate, previously washed with serum-free medium. After 4 h of incubation on a rocking platform at room temperature, 1 ml of complete TC100 medium was added and incubation continued at 28 °C in a humidified environment. Five days later, the medium was harvested, and recombinant virus was plaque-purified by optical screening for plaques with occlusion negative phenotype (Summers and Smith, 1988). After two rounds of purification, the presence of recom-

```
GATCCCAGGCTTTTGCAGAGATCGAGGGTAGACATCACCATCACCATCACTAGT
    GGTCCGAAAACGTCTCTAGCTCCCATCTGTAGTGGTAGTGGTAGTCGATCAGATC
BamHI                Factor Xa      6 × His    STOP XbaI
```

served to generate pBS-hSC:6xHis. This sequence encoding the cleavage site for Factor Xa, six consecutive histidines and a stop codon was inserted downstream of the codon for Glu^{569}.

In order to insert SC sequences into the vaccinia transfer vector p11K (Bertholet *et al.*, 1986), the cDNAs were excised from pBS-hSC and pBS-hSC-6xHis by *EcoRI/XbaI* double digestion, Klenow filled-in, and blunt-end ligated into *BamHI/EcoRI* cut and Klenow filled p11K. Clones carrying the insert in either orientation were recovered for the generation of recombinant vaccinia viruses. The constructs were called p11K-hSC, p11K-hSC$_{rev}$ (reverse orientation), p11K-hSC:6xHis, and p11K-hSC:6xHis$_{rev}$, respectively.

Human SC was also cloned into the vaccinia transfer vector pHGS-1 containing the TAAATG element including the translation start codon from the vaccinia 11K promoter (Bertholet *et al.*, 1985). The 5′ end of the gene was modified using a *ClaI/AccI* fragment generated by recombinant PCR (Higuchi, 1990), using oligonucleotides 5′-AATAATTTT-CGCGCGGCCCATTTATAGCATAGAAA-3′ and 5′-TTTCTATGCTAT-

binant and the absence of wild-type virus was confirmed by PCR as described (Malitschek and Schartl, 1991), using the polyhedrin gene flanking primers 5′-TTTACTGTTTTCGTAACAGTTTTG-3′ (forward) and 5′-CAACAACGCACAGAATCTAG-3′ (reverse).

Production of Recombinant hSC in Mammalian and Insect Cells

Stationary phase CV-1, HeLa, or TK$^-$ 143B cells at a density of 2.0–2.5 $\times$ 10^7 cells/175 cm^2 T-flask in 20 ml of medium were washed with PBS (Sambrook *et al.*, 1989) and infected with recombinant vaccinia virus at the indicated multiplicity of infection (m.o.i.). Trial expression assays were performed with cells cultivated in 6-well dishes in 1 ml of medium. Infected cells were cultured in Dulbecco's modified Eagle's medium in the absence of serum and antibiotics. To assay for secreted hSC, 20–50-μl aliquots of culture medium were removed at defined intervals and replaced by fresh medium in order to avoid changes in the starting culture volume. Culture supernatants originating from cells grown in the absence of virus, infected with wild-type

virus, or infected with recombinant virus carrying the engineered hSC DNA in reverse orientation with respect to the promoter were included as controls.

HeLaS3 cells grown to a density of 6×10^5 cells/ml in suspension minimal essential medium were transferred under sterile conditions to centrifuge bottles, pelleted $120 \times g$ for 10 min at room temperature, then washed twice with PBS and once with serum-free suspension minimal essential medium. After resuspension at a density of 1.0×10^7 cells/ml, they were poured into a spinner bottle, infected with an m.o.i. of 10 for 1 h, diluted to 4×10^5 cells/ml in serum-free suspension minimal essential medium, and then incubated for 21–24 h. Culture supernatant was harvested by centrifugation for 15 min at $120 \times g$.

Baculovirus inocula for infection of Sf9 cells were obtained from cell culture supernatants recovered at least 4 days post-infection at m.o.i.'s larger than 1 with master stock virus. Sf9 cells at densities of 1×10^6 cells/ml in shaker cultures or 5×10^6 cells/25-cm^2 T-flask were infected at estimated m.o.i.'s of 1 or 5 by addition of a corresponding volume of virus inoculum directly to the cultures. Four days post-infection (or as indicated), cells were centrifuged for 10 min at $600 \times g$ and the supernatants containing secreted recombinant protein were harvested. Expression of secreted and intracellular recombinant SC from mammalian or insect cells was monitored by immunoblotting.

Affinity Purification of Recombinant Human Secretory Component

Nickel Chelate Affinity Chromatography—Protein recovered from mammalian cell culture medium was dialyzed/concentrated (100-fold) in 20 mM sodium phosphate, 500 mM NaCl, pH 7.8 (Ni^{2+} binding buffer), in a Spectrum Micro-ProDiCon system model FS-15 using 25-kDa molecular weight cut-off membranes. This material was applied to a Hi-trap chelating matrix (Pharmacia Biotech; 1-ml bed volume/ml of concentrated culture supernatant), charged with nickel ions and equilibrated with Ni^{2+} binding buffer. Culture supernatants originating from infected Sf9 cells were loaded three times onto Ni^{2+}-nitrilotriacetic acid-agarose columns (Qiagen; 300-μl bed volume for 1 ml of culture supernatant for analytical, and 2-ml bed volume per 100 ml of supernatant for preparative assays), equilibrated with Ni^{2+} binding buffer. Columns were subsequently washed with 20 mM sodium phosphate, 500 mM NaCl, pH 6.3 (Ni^{2+} washing buffer), followed by the same buffer containing 20 mM imidazole. Bound protein was eluted with washing buffer containing 100 mM imidazole and fractions were collected in siliconized polypropylene tubes. Eluted proteins were subjected to SDS-PAGE, and purity as well as lack of degradation were assayed by silver staining and immunoblotting.

Concanavalin A Affinity Chromatography—Mammalian cell culture supernatant were dialyzed and concentrated as above, in 10 mM Tris-HCl, 150 mM NaCl, 1 mM $CaCl_2$, 1 mM $MnCl_2$ (ConA-binding buffer). This material or unconcentrated insect cell culture supernatant were passed over ConA-agarose beads (Vector Laboratories, 500-μl bed volume per ml of loaded material), equilibrated with ConA binding buffer. The columns were extensively washed with ConA binding buffer, and bound material was eluted with the same buffer containing 500 mM methyl-α-D-mannopyranoside (Fluka). Collection and subsequent analysis of fractions were carried out as above.

Enzymatic Deglycosylation

Recombinant hSC produced in various host cell types was treated with the endoglycosidases PNGase F (EC 3.2.2.18 and 3.5.1.52) or EndoH (EC 3.2.1.96; both Boehringer Mannheim) according to the manufacturer's instructions. Briefly, 150 μl (insect) or 600 μl (mammalian) cell culture supernatant or, as controls, appropriate amounts of human sIgA (Sigma) or purified nonglycosylated hSC produced in bacteria, were extracted with a mixture of methanol and chloroform and precipitated with methanol, as described (Wessel and Flügge, 1984). The precipitates were solubilized and denatured by boiling for 2 min in 50 μl of 1% SDS. 15 μl of this solution were added to 135 μl of PNGase F buffer (20 mM sodium phosphate, 50 mM EDTA, 10 mM sodium azide, 0.5% Nonidet P-40, 0.1 M β-mercaptoethanol, pH 7.2) for mock treatment and PNGase F digestion, or to 135 μl of the same buffer, but adjusted to pH 5.5, for EndoH digestion. The samples were again boiled for 2 min, then 4 μl of PNGase F (0.2 unit/μl), EndoH (1 milliunit/μl), or H_2O were added to the corresponding tube. Digestions and control samples were incubated at 37 °C for 16 h, then extracted and precipitated using the methanol/chloroform procedure. The resulting pellets were dissolved in sample buffer for analysis by immunoblotting.

Immunoblotting

Proteins were subjected to PAGE on 6 or 8% resolving gels under denaturing (0.1% SDS) and reducing (100 mM dithiothreitol) conditions, together with prestained molecular weight markers (Bio-Rad). Separated proteins were then transferred to nitrocellulose or polyvinylidine difluoride membranes (Bio-Rad) according to the manufacturer's recommendations. Nonspecific binding sites were saturated for 1 h at room temperature by incubation in a blocking buffer made of TBS (25 mM Tris-HCl, 137 mM NaCl, 2.7 mM KCl, pH 7.5), 5% non-fat dry milk, and 0.05% Tween 20 (Bio-Rad). The membrane was probed for 1 h at room temperature with either a rabbit antiserum against recombinant hSC[2] or a mouse monoclonal antibody to hSC (Sigma), diluted 1:3,000. Bound antibodies were detected using horseradish peroxidase-conjugated anti-rabbit or anti-mouse immunoglobulin antibodies (Sigma) and the enhanced chemiluminescence kit from Amersham.

Dot Blot Reassociation Assay

Dimeric IgA specific for mouse mammary tumor virus gp52 protein were purified from mouse hybridoma clone MB2 (Weltzin *et al.*, 1989) by size exclusion chromatography on a Superose CL-4B column (2.2 × 100-cm; Pharmacia Biotech Inc.). Mouse IgG were obtained from Sigma. Binding of recombinant hSC to dIgA antibodies was tested as follows. 500 ng of mouse dIgA, or as a control 200 ng of mouse IgG in 10 μl of PBS containing 6.25% glycerol, were spotted onto 24-mm diameter nitrocellulose membranes (0.2-μm pore size; Schleicher & Schuell) and allowed to air dry. Filters were then transferred to 6-well tissue culture dishes and blocked with TBS containing 5% non-fat dry milk and 0.05% Tween 20 for 1 h at room temperature. After removal of the blocking solution, the dIgA-carrying filters were overlaid with 100 ng of recombinant hSC protein (recovered from crude culture supernatant, or purified by affinity chromatography) in 1.5 ml of fresh blocking solution for 1 h at room temperature. After three 10-min washes with TBS, 0.05% Tween 20, recombinant hSC bound to the dIgA on the membranes was detected using monoclonal anti-hSC antibodies (Sigma) under the conditions given for immunoblotting. Similarly, samples of recombinant hSC containing 100 ng of protein were immobilized onto nitrocellulose and overlaid with mouse dIgA or IgG under the conditions given above. Detection of the bound component was performed with anti-mouse IgA or anti-mouse IgG Fc specific-monoclonal antibodies (Sigma), respectively.

ELISA

Two-antibody sandwich assay was performed according to Harlow and Lane (1988). The first antibody was mouse monoclonal antibody to hSC (Calbiochem) at a dilution of 1:500, the second antibody was rabbit polyclonal antiserum to hSC[2] used at a dilution of 1:1,000, and detection was carried out using a goat anti-rabbit IgG peroxidase conjugate antibody (Sigma; dilution of 1:1,000) with 1,2-phenylenediamine as the chromogene. These conditions were optimized to detect as little as 0.25 ng of hSC in a native conformation.

High Pressure Gel Filtration Chromatography

In a total volume of 100 μl of PBS, varying amounts of purified recombinant hSC were incubated with a constant amount of dimeric IgA, yielding solutions of 0.5:1, 1:1, and 2:1 μM, respectively. The solutions were incubated for 16 h at ambient room temperature and then passed over a 1-cm × 30-cm Superose 12 HR 10/30 column (Pharmacia) coupled to a FPLC system (Pharmacia) at 0.3 ml/min. Elution was effected with PBS, with continuous monitoring performed at 278 nm. The presence of dimeric IgA and recombinant SC in peak fractions was confirmed by Western blotting.

RESULTS

Construction of Recombinant Virus—In order to determine the role of SC in IgA antibody stability and its contribution to protection against microbial pathogens, we have produced recombinant human SC that retains its capacity to bind dimeric IgA using two viral expression systems. Since SC is generated by proteolytic cleavage of the pIgR during transepithelial transport we introduced a stop codon in the receptor's cDNA at a position corresponding to the putative natural cleavage site. The 5′ region encoding the hSC signal peptide was preserved in order to direct the protein into the secretory pathway and to

[2] L. Rindisbacher and B. Corthésy, unpublished data.

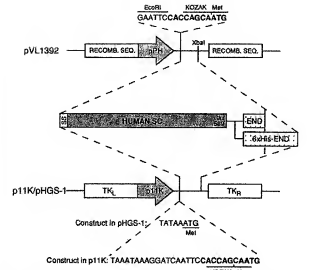

FIG. 1. **Schematic representation of cloning and engineering of hSC sequence into baculovirus and vaccinia virus expression vectors.** The pVL1392 construct contains the hSC cDNA fragment encoding amino acid Met^1 to Glu^{589} downstream of the baculovirus polyhedrin promoter (*pPH*). A stop codon (*End*) or an artificial sequence coding for 6 histidines and a stop codon (*6xHisEnd*) was introduced 3′ of amino acid 589. The naturally occurring Kozak sequence in hSC was conserved in the cloning process. Constructs p11K and pHGS1 contain the same segment of hSC cDNA, with the presence or absence of codons for a 6xHis tail. Both constructs are under the control of the vaccinia virus late 11K promoter (*p11K*). Construct p11K carries the hSC Kozak sequence, while in construct pHGS1, the highly conserved vaccinia virus promoter element TAAATG) is coupled to the initiation ATG codon as in the natural situation. At the level of the junctions between viral and hSC sequences, the hSC 5′ region is shown in *bold* characters. Sequences involved in homologous recombination are depicted as *open rectangles*, promoters as *dot-filled arrows*, and the ss box upstream of the hSC gene stands for signal sequence.

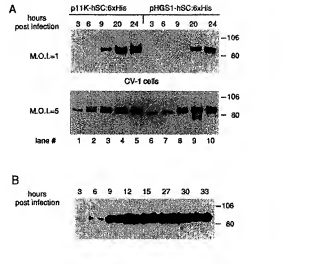

FIG. 2. **Time course of hSC expression in mammalian and insect cells as a function of multiplicity of infection.** *Panel A*, cultures of CV-1 cell monolayers were infected either with vaccinia virus recombinant p11K-hSC:6xHis (*lanes 1–5*) or vaccinia virus recombinant pHGS1-hSC:6xHis (*lanes 6–10*) at m.p.i. of 1 plaque forming unit/cell (*top*) and 5 plaque forming units/cell (*bottom*). At 3, 6, 9, 20, and 23 h post-infection, aliquots were taken up, separated by SDS-PAGE (8% separating gel; reducing conditions), transferred to blotting membrane, and hSC was detected immunochemically as described under "Experimental Procedures." Molecular size markers are given in kiloDaltons. *Panel B*, refined time course analysis of hSC expression in HeLa cells infected with vaccinia virus recombinant p11K-hSC:6xHis at a m.o.i. of 5 plaque forming units/cell. Aliquots of supernatant were collected 3, 6, 9, 12, 15, 27, 30, and 33 h post-infection. Protein accumulation in the culture medium was monitored using Western blot. *Panel C*, analysis of hSC synthesis during recombinantbaculovirus infection. Sf9 cell grown in suspension (*lanes 1–6*) or as monolayers (*lanes 7–12*) were infected with approximately 1 and 5 plaque forming units/cell of baculovirus recombinant pVL1392-hSC:6xHis. Culture medium of cells grown in suspension or as a monolayer were taken up at day 0, 1, 2, 3, 4, and 5, and analyzed by immunodetection.

subsequently recover the recombinant protein from the culture medium. Finally, to facilitate the purification of the protein, a histidine hexamer tag preceded by a factor Xa cleavage site was inserted upstream of the artificial stop codon, encoding six consecutive histidines preceeded by a Factor Xa cleavage site. The resulting recombinant genes were subcloned into vaccinia and baculovirus transfer vectors (Fig. 1).

The foreign DNA was introduced into the double-stranded DNA genome of vaccinia or baculovirus following published procedures (Mackett *et al.*, 1984; Summers and Smith, 1988). The foreign genes require viral promotors to drive efficient transcription. The transfer plasmids p11K and pHGS-1 contain the vaccinia late promoter P11K (Hänggi *et al.*, 1986) flanked by vaccinia TK sequences to direct recombination into the TK locus of the viral genome. In the p11K recombinants, the Kozak sequence (Kozak, 1986) was derived from the hSC gene itself, while pHGS-1 recombinants contain viral transcriptional and translational regulatory sequences originating from the 11K viral gene. Recombinant hSC DNAs containing their own translation initiation signals were subcloned into the baculovirus transfer vector pVL1392, downstream of the promoter governing expression of the viral polyhedrin gene. The presence of the hSC cDNA insert in the viral genomes, as well as the absence of contaminating wild-type virus, was ascertained by PCR utilizing hSC sequence- or transfer vector-specific primers, respectively, that generated unique amplification products of the expected sizes (data not shown).

Optimization of Recombinant Human Secretory Component Expression—We first determined the kinetics of hSC production after infection at a multiplicity of infection (m.o.i.) of 1 or 5. CV-1 cells were infected with recombinant vaccinia viruses p11K-hSC:6xHis and pHGS1-hSC:6xHis. To facilitate subsequent purification of the product, the cells were cultured in serum-free Dulbecco's modified Eagle's medium during infection and the production phase. Aliquots of culture supernatant were removed at 3, 6, 9, 20, and 23 h post-infection, separated by polyacrylamide gel electrophoresis, and immunoblotted with hSC antiserum. The recombinant protein appeared 9 h after infection using the p11K-hSC:6xHis recombinant virus (Fig. 2*A*). Increasing the m.o.i. from 1 to 5 accelerated the production without increasing the final yield of hSC by 20 and 24 h after infection (Table I). Addition of serum to the culture medium did not enhance SC production (data not shown).

The kinetics of hSC production reflected that observed with other heterologous cDNAs driven by the vaccinia late promoter (Hänggi *et al.*, 1986). To test whether the rate of hSC production and secretion observed in CV-1 cells was similar in another cell line, we infected HeLa cells at an m.o.i. of 5 with the

TABLE I

Production of recombinant hSC using the vaccinia virus system.

Serial dilutions of culture supernatants were assayed by ELISA using purified sIgA as a standard. The linear part of the response curve was used for quantification.

Recombinant vaccinia virus	Cell line	Time post infection	m.o.i.	hSC (μg/ml supernatant)
		h		
p11K-hSC:6xHis	CV-1	20	1	8.6
p11K-hSC:6xHis	CV-1	20	5	8.9
pHGS1-hSC:6xHis	CV-1	20	1	6.4
pHGS1-hSC:6xHis	CV-1	20	5	6.3
p11K-hSC:6xHis	CV-1	24	1	9.0
p11K-hSC:6xHis	CV-1	24	5	9.0
pHGS1-hSC:6xHis	CV-1	24	1	6.4
pHGS1-hSC:6xHis	CV-1	24	5	6.5
p11K-hSC:6xHis	HeLa	3	5	
p11K-hSC:6xHis	HeLa	6	5	0.9
p11K-hSC:6xHis	HeLa	9	5	5.4
p11K-hSC:6xHis	HeLa	15	5	7.9
p11K-hSC:6xHis	HeLa	27	5	9.0
p11K-hSC:6xHis	HeLa	30	5	9.3
p11K-hSC	CV-1	20	1	8.8
p11K-hSC:6xHis(A)	CV-1	20	1	8.3
pHGS1-hSC	CV-1	20	1	6.2
pHGS1-hSC:6xHis(A)	CV-1	20	1	6.1

p11K-hSC:6xHis recombinant virus, and looked for hSC production at shorter intervals. The appearance of hSC was assessed by immunoblotting (Fig. 2*B*), and quantitative analysis was based on ELISA (Table I). Secreted recombinant hSC could be observed 6 h after infection, starting to accumulate after 9 h.

Following infection of insect cells with recombinant baculovirus, expression of the corresponding recombinant protein is known to follow slower kinetics when compared to vaccinia virus (Summers and Smith, 1988). Similar slow kinetics of hSC secretion were observed in Sf9 cells infected with pVL1392-hSC:6xHis recombinant baculovirus (Fig. 2*C*). Suspension or monolayer cultures were infected at estimated m.o.i.s of 1 and 5, and aliquots of culture medium were removed at 0 through 5 days post-infection in 24-h intervals and analyzed by immunoblotting. Suspension cultures start to accumulate recombinant protein in the supernatant 2 days post-infection. As compared to monolayer cultures, production in suspension yielded higher amounts of hSC.

On immunoblots, recombinant hSC produced from recombinant vaccinia virus was detected in as little as 2.5 μl of cell culture supernatant, whereas the baculovirus product was revealed in less than 1 μl of supernatant. The protein expressed by each of the systems was quantitated densitometrically by comparing the signals obtained from increasing amounts of culture supernatant with known quantities of an sIgA standard on the linear part of the response curve of the Western blot (data not shown). The concentration of hSC recovered in culture supernatants from the vaccinia virus/mammalian cell system ranged from 5 to 10 mg/liter, while the baculovirus/insect cell system yielded up to 50 mg/liter.

Addition of Sequences to the COOH Terminus of hSC Does Not Alter Expression—The cDNAs introduced into the viral genomes contained initiation sites for translation derived either from the hSC gene itself or, in the case of vaccinia pHGS-1 recombinants, from the viral 11K gene. In addition, a 6xHis tag preceded by a Factor Xa cleavage site were fused to the artificial carboxyl termini of the recombinant proteins (Fig. 1). To determine whether these minor differences in nucleotide and amino acid sequence altered hSC expression, CV-1 cell monolayers were infected with the various vaccinia virus recombinants at an m.o.i of 1. Twenty hours post-infection, equal

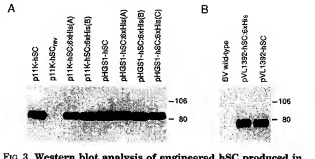

FIG. 3. **Western blot analysis of engineered hSC produced in CV-1 and Sf9 cells.** *Panel A*, expression of hSC as a function of engineered cDNA inserts. CV-1 cell monolayers were infected either with recombinant vaccinia virus p11K-hSCEnd, vaccinia virus recombinant p11K-hSC$_{myc}$, two individual vaccinia virus recombinants p11K-hSC:6xHis, recombinant vaccins virus pHGS1-hSC, three individual vaccinia virus recombinants pHGS1-hSC:6xHis at a multiplicity of 1 plaque forming unit/cell. 20 h post-infection, cell culture media were collected and 20 μl of each supernatant were analyzed by immunoblotting as described under "Experimental Procedures." Molecular size markers are given in kDa. *Panel B*, expression of hSC carrying or lacking a 6xHis tag in Sf9 cells infected for 4 days with baculovirus recombinant pVL1392-hSC or pVL1392-hSC:6xHis, respectively. No expression of hSC occurs in Sf9 cells infected with wild type BV.

amounts of supernatant were collected, and the presence of hSC protein was assessed by Western blotting. As shown in Fig. 3*A*, comparable signal intensities on the Western blot and similar patterns of migration of recombinant hSC production were observed. With both the hSC and 11K regulatory sequences upstream of the ATG codon, equivalent amounts of protein were synthesized as assayed by ELISA (Table I), reflecting comparable translation initiation efficiencies. The addition of six histidyl residues together with the target sequence for Factor Xa at the carboxyl terminus of the protein did not alter the secretion of recombinant hSC using either viral expression systems (Fig. 3, *A* and *B*). No hSC production was detected when CV-1 cells were infected with a vaccinia recombinant carrying the hSC gene in reverse orientation with respect to the viral promoter. Accordingly, no recombinant protein was produced by CV-1 or Sf9 infected with wild-type virus or by non-infected cells (data not shown).

The Glycosylation Pattern of hSC Differs Depending on the Cell Line and the Recombinant Viral Expression System—The apparent molecular weight of secreted recombinant hSC varied significantly depending on the host cell type used for expression (Fig. 4*A*). When produced in insect cells which are unable to generate fully *glycosylated* forms, the baculovirus hSC product migrated faster than natural hSC on SDS gels. When recovered from human HeLa or TK$^-$ 143B cells, hSC significantly and reproducibly migrated at a slightly higher M_r than natural human SC, or recombinant hSC produced by monkey CV-1 cells. In order to correlate these size differences with glycosylation, we examined the susceptibility of recombinant hSC to the action of endoglycosidase PNGase F, which removes high mannose, hybrid, and complex type *N*-linked carbohydrates from glycoproteins (Tarentino and Plummer, 1994). Upon PNGase F treatment, two bands were observed with recombinant hSC produced in mammalian cells (Fig. 4*B*); a 66-kDa band comigrating with the unglycosylated bacterial product, and a 60-kDa band corresponding to the deglycosylated "natural" product. In Sf9 insect cells, only the 60-kDa band could be detected. We explain this digestion pattern as follows. Following transcytosis, the pIgR is trimmed of both its transmembrane and cytoplasmic domains by a so far unidentified protease activity, leading to the release of SC. The site of protease cleavage has not been defined with dependable accuracy. Our constructs are based on cleavage at Glu^{599} (see

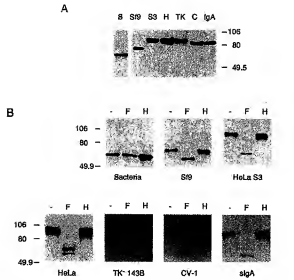

FIG. 4. **Enzymatic deglycosylation of recombinant hSC expressed in different cell lines.** *Panel A*, whole cell lysate from *E. coli* M15 strain transformed with expression vector pQE9-hSC6xHisEnd (*B*), crude supernatants from baculovirus recombinant pV1.1392-hSC: 6xHis-infected Sf9 cells (*Sf9*), vaccinia virus recombinant p11K-hSC: 6xHis-infected HeLaS3 cells (*S3*), HeLa cells (*H*), TK- 143B cells (*TK*), CV-1 cells (*C*), and standard human secretory IgA (*IgA*) were separated on a reducing 8% SDS-polyacrylamide gel, blotted to polyvinylidine difluoride membrane, and location of hSC was identified using anti-hSC monoclonal antibody. Note the difference in the patterns of migration of the overproduced hSC proteins compared to the natural hSC. *Panel B*, supernatants shown in *panel A* were incubated in the presence of PNGase F (*F*), endoglycosydase H (*H*), or the corresponding buffer alone (−). The resulting samples were electrophoresed on 6% polyacrylamide gel, and processed for immunodetection.

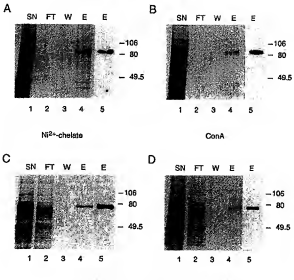

FIG. 5. **Purification of recombinant hSC by affinity chromatography.** Analysis by SDS-PAGE (8% separating gel, reducing conditions) of purified hSC produced either in HeLaS3 cells infected with vaccinia virus recombinant p11K-hSC:6xHis (*panels A* and *B*), and in Sf9 cells infected with baculovirus recombinant pV1.1392-hSC:6xHis (*panels C* and *D*). *Panels A* and *C* correspond to samples resulting from affinity chromatography on Ni^{2+}-chelate column, whereas *panele B* and *D* contain fractions from the ConA affinity column. Samples in *panels A–D* were loaded in the following order: *lane 1*, cell culture supernatant (*SN*); *lane 2*, column flow-through (*FT*); *lane 3*, column fraction containing the first wash (*W*); *lanes 4* and *5*, column fraction containing the elution peak of hSC (*E*). Proteins were visualized by silver staining (*lanes 1–4*) and immunodetection (*lane 5*). Molecular size markers are given in kiloDaltons (kDa).

"Experimental Procedures"), leading to the synthesis of a recombinant protein with a calculated molecular mass of 66,026 daltons in the absence of any glycosylation. Assuming that the band at 60-kDa represents the deglycosylated, naturally cleaved pIgR, a portion of the hSC proteins expressed in mammalian cells and all of the protein produced in insect cells have somehow been trimmed to the size of natural hSC. On the other hand, a proportion of the mammalian products remains intact and migrates at the expected position for a fully deglycosylated recombinant hSC, such as the unglycosylated recombinant bacterial product. Such proteolytic cleavage within the COOH-terminal region of the recombinant protein would also remove the 6 x histidine tag, thus affecting the yield of hSC purified on Ni^{2+} affinity resins (see below). Endoglycosidase H, an enzyme that does not cleave complex type *N*-linked carbohydrate (Elbein *et al.*, 1982), did not induce any significant change in the molecular weight of recombinant hSC (Fig. 4*B*), suggesting that the bulk of carbohydrates *N*-linked to recombinant hSC is of the complex type.

Purification of Recombinant Human Secretory Component—Recombinant hSC protein carrying a carboxyl-terminal 6xHis tag produced by HeLaS3 or Sf9 cells maintained in serum-free medium was purified from 20-h or 4-day post-infection supernatants, respectively, by Ni^{2+}-chelate affinity chromatography. Small volumes of about 100-fold concentrated HeLa or unconcentrated Sf9 supernatant were applied onto equilibrated in binding buffer at pH 8.0. In order to remove unspecifically bound material, the column was washed stepwise with washing buffer (pH 6.3), and subsequently with washing buffer containing a subelution concentration (20 mM) of imidazole competitor. Recombinant hSC was eluted at 100 mM imidazole, indicating high binding specificity to the Ni^{2+} resin. Purified hSC from Sf9 cells migrated on SDS-PAGE as a single band of about 70 kDa (Fig. 5*C*, *lane 4*) with no degradation products as revealed by immunodetection (Fig. 5*C*, *lane 5*) and the recovery was estimated to be 80–90% of the amount of recombinant hSC loaded onto the column. The recovery of purified hSC produced using the vaccinia system reached almost 100% with several SC-unrelated proteins probably of viral origin contaminating the preparation (Fig. 5*A*, *lanes 4* and *5*).

This drawback prompted us to evaluate a different affinity chromatography protocol. Since recombinant hSC produced in mammalian and Sf9 cells is glycosylated (Fig. 4), we explored the possibility of purifying the recombinant protein on a lectin column. Dialyzed/concentrated CV-1 supernatant or unconcentrated Sf9 supernatant were loaded onto the ConA column and, after extensive washing, recombinant hSC was eluted with 0.5 M methyl-α-D-mannopyranoside. Human SC produced by the vaccinia/HeLaS3 system eluted as a single M_r 85,000–90,000 band on silver-stained SDS-PAGE (Fig. 5*B*, *lane 4*) or immunoblot (Fig. 5*B*, *lane 5*). The recovery was over 90%. The protein expressed in Sf9 cells was also efficiently purified (Fig. 5*D*), but the elution was over a broader range of fractions with a final recovery below 60%

Interaction Between Recombinant hSC and Dimeric IgA—The IgA binding activity of recombinant SC was assessed by a dot blot reassociation assay (DORA). The principle illustrated in Fig. 6*A* is described under "Experimental Procedures." After immobilization of one of the interacting partners on a nitrocellulose filter, the other component is added as an overlay in a buffered solution in the presence of nonspecific protein competitor. Association is determined by immunodetection of the component in the overlay phase. Formation of a specific SC·dIgA complex was observed with hSC recovered from the superna-

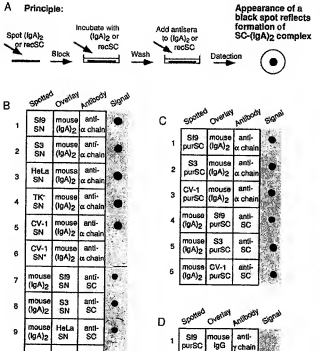

FIG. 6. ***In vitro* determination of binding specificity between recombinant SC and dimeric IgA.** *Panel A*, cartoon representation of DORA. Details are given under "Experimental Procedures." *Panel B*, binding of mouse dimeric IgA ($(IgA)_2$ to human SC secreted in culture supernatant (*SN*) of recombinant virus-infected cells (*lanes 1–6*). Sf9 cells were infected with baculovirus recombinant pVL1392-hSC:6xHis, and mammalian cells with vaccinia virus recombinant p11K-hSC: 6xHis. *SN** corresponds to supernatant of CV-1 cell infected with vaccinia virus recombinant p11K-hSC:6xHis$_{rev}$. *Lanes 7–12* show binding of the same set of SC-containing SN to spotted dIgA. SC and dIgA were present at a 1:1 molar ratio. *S3*, HeLaS3 cells; *anti-α-chain*, affinity purified antibody against the heavy chain of mouse IgA; *anti-SC*, monoclonal antibody against human SC. *Panel C*, binding of dIgA to purified recombinant SC produced in culture SN of Sf9, HeLaS3, and CV-1 cells infected as for the experiments in *panel B* (*lanes 1–3*). Association between purified SC and immobilized dIgA is shown in *lanes 4–6*. *Panel D*, lack of interaction between purified recombinant SC produced in virus-infected Sf9 and HeLaS3 cells and mouse IgG (*lanes 1* and *2*). Binding of anti-SC antibody to spotted SC is not abolished after incubation with IgG (*lane 3*). Anti-γ-chain, affinity purified antibody against the Fc domain of mouse IgG.

tant of insect and mammalian cells infected with the appropriate recombinant virus (Fig. 6*B*, *lanes 1–5* and *7–11*). Both interacting partners retained their binding capacity indicating that the functional structure of the immobilized protein was preserved. This was further supported by the recognition of recombinant SC by SC-specific antibodies (Fig. 6*D*, *lane 3*). No binding was detected in supernatants from cells infected with recombinant vaccinia expressing SC in the reverse orientation (p11K-hSC:6xHis$_{rev}$; Fig. 6*B*, *lanes 6* and *12*), with wild-type virus or from non-infected cells (data not shown). In order to further demonstrate the specificity of the interaction, we repeated the DORA with purified hSC produced in three different cell lines (Fig. 6*C*). Consistently, immobilized SC bound dimeric IgA (*lanes 1–3*) and recombinant hSC bound to immobilized dimeric IgA (*lanes 4–6*). Recombinant SC did not bind IgG (Fig. 6*D*, *lanes 1* and *2*). To determine which proportion of

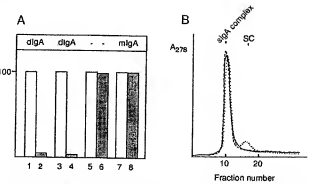

FIG. 7. ***In vitro* determination of binding efficiency between recombinant SC and dimeric IgA.** *Panel A*, over 95% of recombinant hSC input binds dimeric IgA (*dIgA*). DORA was performed as described under "Experimental Procedures," and unbound hSC in the supernatant was analyzed by ELISA. *Lanes 1*, *3*, *5*, and *7*, input hSC; *lanes 2*, *4*, *6*, and *8*, hSC in the overlay after a 1-h incubation. *Lanes 1* and *2*, hSC expressed in Sf9 cells and dIgA; *lanes 3* and *4*, hSC expressed in HeLa cells and dIgA; *lanes 5* and *6*, hSC expressed in HeLa cells and no dIgA; *lanes 7* and *8*, hSC expressed in HeLa cells and monomeric IgA (*mIgA*). The ELISA read-out corresponding to unbound hSC is expressed as 100% on the *vertical axis*. *Panel B*, high pressure gel filtration chromatography of varying ratios of recombinant hSC to dIgA. The reactants were present at a 0.5:1 molar ratio (—), a 1:1 molar ratio (- - -), and a 2:1 molar ratio (···) of hSC to dimeric IgA, respectively. The position of the sIgA complex and free SC are indicated on the *top* of the peaks.

recombinant hSC is capable of associating with dimeric IgA, we analyzed by ELISA the hSC recovered in the overlay after incubation with the nitrocellulose filters carrying the polymeric immunoglobulins (Fig. 7*A*). No more than 5% of the recombinant hSC protein input can be detected when an equimolar mixture of the partners is mixed (compare *lanes 1* and *3* with *lanes 2* and *4*), reflecting both quantitative binding to dimeric IgA and correct three-dimensional folding. In the absence of dimeric IgA (*lane 6*), or when monomeric IgA was spotted (*lane 8*), recombinant hSC remained free in the overlay. These series of binding data demonstrate the usefulness of the DORA test for rapid and sensitive assessment of SC·dIgA reassociation *in vitro*.

SC·dIgA complex formation was further demonstrated by high pressure gel filtration chromatography experiments. Different molar ratios of recombinant hSC and dimeric IgA were reacted at room temperature for 16 h, and their products were resolved by size fractionation (Fig. 7*B*). Observation of a shift in the position of elution of hSC to that of dimeric IgA indicates that the two proteins can recognize each other in this dynamic assay totally performed in buffered solution. At a 0.5:1 ratio of hSC to IgA, only the high molecular weight complex peak is present, indicating that the reformation of hSC·IgA complex occurs, and accordingly, that recombinant hSC is properly folded. At a 1:1 ratio, the hSC peak is again totally shifted to the position of the high molecular mass species. At a 2:1 ratio, the hSC·IgA complex peak remains the same, but a free hSC peak is now observed.

DISCUSSION

Secretory IgA, the major immunoglobulin class in mucosal and glandular secretions, consists of one dimeric IgA unit and two additional polypeptide chains, J chain and SC. The heavy, light, and J chains are synthesized and dimeric IgA is assembled in plasma cells, whereas SC is contributed by the epithelial cells of mucosal and glandular tissues. To produce large amounts of sIgA for passive oral (mucosal) immunization (Apter *et al.*, 1993a, 1993b; Lee *et al.*, 1994), it is necessary to synthesize both SC and dimeric IgA in different cells and

subsequently properly associate the two components. While large amounts of dIgA can be produced by and purified from hybridoma clones, preparation of complete sIgA has been so far prevented by the lack of efficient production systems for SC. As a first step toward *in vitro* reconstitution of sIgA antibody molecules, we evaluated two viral expression systems for the production of human SC that retains its capacity to bind and stabilize dimeric IgA molecules.

The insect cell-based baculovirus system is well suited for high-level expression of heterologous genes (Miller, 1993). Appropriate folding, assembly, and targeting of recombinant proteins by insect cells, as well as their capacity to perform many of the post-translational modifications of higher eukaryotes, usually allowed the recovery of large amounts of biologically active product. Complex molecular structures such as murine immunoglobulin heterodimers have been successfully produced utilizing this system (Putlitz, 1990). Vaccinia virus has been used to express foreign genes in mammalian cells for more than 10 years (Mackett *et al.*, 1982; Panicali and Paoletti, 1982). Due to the extended host range of vaccinia, the heterologous gene contained in one single virus recombinant can be expressed in almost any mammalian cell type. Therefore, infection with recombinant vaccinia virus usually generates high amounts of a mammalian protein that most closely resembles its natural counterpart in terms of structure and function.

We first established that recombinant SC was produced and transported along the secretion pathway in both systems. The levels of expression for all constructs were indistinguishable and within the expected range, *i.e.* 5–10 mg of protein/liter of culture medium for the vaccinia system, and 50 mg of protein/liter of culture medium for the baculovirus system. In addition, the use of translation initiation sites of different origins in the vaccinia system did not have any visible effect either. Thus, subtle modifications in the engineered cDNA were very well accommodated by the cellular machinery responsible for transcription, translation, maturation, and secretion of recombinant hSC.

Human SC purified from milk is heavily glycosylated with four *N*-linked sugar side chains accounting for over 20% of its molecular weight (Mizoguchi *et al.*, 1982). A major disadvantage of the baculovirus system compared to the mammalian cell-based system is its limited ability to terminally glycosylate glycoproteins (Miller, 1993, and references therein). Our results with endoglycosidase treatment indicate that complex-type carbohydrate contributes approximately 10 and 19–24 kDa to the apparent molecular mass of hSC produced in insect and mammalian cells, respectively. hSC from purified sIgA antibodies behaves in a very similar fashion as the recombinant proteins in terms of migration on SDS-PAGE, as well as toward treatment with endoglycosidases, indicating a strong structural relationship between the natural and overproduced species. Recombinant SC produced by insect and mammalian cells were both able to efficiently bind to dimeric IgA, suggesting that slight differences in glycosylation did not affect the interaction, as previously reported by Bakos *et al.* (1991, 1994). Indeed, these authors showed that deglycoeylated SC bound with equal or higher affinity to polymeric IgAs. Whether glycosylation affects the kinetics of SC-IgA association and play a role in protection will require further biochemical and immunological investigations.

Metal-chelate affinity chromatography first described by Porath *et al.* (1975) is based on the ability of certain amino acids (histidine, tryptophan, and tyrosine) to act as electron donors for reversible binding to transition metal ions immobilized on a solid support. The affinity of histidine residues for immobilized Ni^{2+} ions allows selective purification of proteins containing a stretch of at least six consecutive histidines in surface-exposed regions of the molecule, such as amino and carboxyl termini (Hochuli *et al.*, 1987). Fusion of six histidines adds only 720 daltons to the protein, and its biological function and immunogenic properties are usually retained (Janknecht *et al.*, 1991; Parvin *et al.*, 1992; Taussig *et al.*, 1993). Efficient single-step purification of baculovirus-expressed hSC with dimeric IgA binding capability further demonstrates the potential of this chromatography. In contrast, hSC protein expressed with the vaccinia system could not be purified to homogeneity as contaminating polypeptides were repeatedly co-eluted at high imidazole concentration. Since the same pattern of contaminants was observed with different cell lines, it is likely that those are of vaccinia viral origin.

ConA affinity chromatography represents a second efficient single-step procedure to purify recombinant hSC. This was facilitated by growing the cells in serum-free conditions. In addition, it appears that glycoproteins secreted by infected cells represents a small proportion of the large number of cellular and viral proteins present in cell culture supernatants (Fig. 5). The recovery of vaccinia-produced hSC is almost complete, whereas baculovirus-expressed hSC is only partially yielded under identical conditions, reflecting a stronger affinity for the lectin due to the lower content of complex sugars in insect cells rendering more terminal α-D-mannose residues accessible to immobilized ConA.

We have developed a simple dot blot overlay assay to assess IgA binding of recombinant hSC (Fig. 6*A*). The recombinant hSC protein binds exclusively to dimeric IgA, and is produced in an active conformation, as less than 5% is found not to be reassociated with IgA (Fig. 6, *B* and *C*; Fig. 7*A*). The specificity of binding is further illustrated in control experiments showing that hSC does not bind to IgG (Fig. 6*D*). It is worth mentioning at this point of the discussion that we only used purified dimeric IgAs, and not simply the secretion products of hybridoma cultures known to contain monomers, multimers, aggregates, and serum proteins that could nonspecifically trap recombinant hSC in the assay. In addition, the quantitative shift in the position of elution of recombinant hSC upon binding to dimeric IgA observed in gel filtration experiments (Fig. 7*B*) further validates the filter binding assay as a fast, *qualitative*, and reliable test. These binding data indicate that, (*a*) specific recognition between recombinant hSC and dimeric IgA occurs in solution, (*b*) confirm that all, or nearly all the recombinant hSC protein is competent for binding to dimeric IgA, (*c*) argue in favor of an 1:1 stoichiometry of association, as suggested by previous studies (Kerr, 1990). The biochemical nature and kinetics of the interaction of heterologous and homologous IgA with recombinant hSC produced by the different expression systems and cell types is currently being analyzed.

In conclusion, the baculo- and vaccinia viral systems are suitable to provide high yields of recombinant hSC. Efficient procedures allowed purification of the recombinant protein in a single step. This material will be used on a preparative scale for reassociation with mouse and human monoclonal IgA, as well as with humanized recombinant antibodies of the A isotype. This approach will allow investigation *in vitro* of the stabilizing effect of hSC in sIgA complex against protease degradation as well as its contribution to mucosal immune protection (Boren *et al.*, 1993). In addition, thanks to the availability of sufficient amounts of SC, it will be possible to determine in animal models the immunoprotective potential offered by dimeric IgA alone and reconstituted with recombinant SC.

REFERENCES

Apter, F. M., Michetti, P., Winner, L. S., III, Mack, J. A., Mekalanos, J. J., and Neutra, M. R. (1993a) *Infect. Immun.* **61**, 5279–5285
Apter, F. M., Lencer, W. I., Finkelstein, R. A., Mekalanos, J. J., and Neutra, M. R.

(1993b) *Infect. Immun.* **61**, 5271–5278
Bakos, M.-A., Kurosky, A., and Goldblum, R. M. (1991) *J. Immunol.* **147**, 3419–3426
Bakos, M.-A., Widen, S. G., and Goldblum, R. M. (1994) *Mol. Immunol.* **31**, 165–168
Bertholet, C., Drüllien, R., and Wittek, R. (1985) *Proc. Natl. Acad. Sci. U. S. A.* **82**, 2096–2100
Bertholet, C., Stocco, P., Van Meir, E., and Wittek, R. (1986) *EMBO J.* **5**, 1951–1957
Boren, T., Falk P., Roth, K. A., Larson, G., and Normark, S. (1993) *Science* **262**, 1892–1895
Brandtzaeg, P. (1989) *Curr. Top. Microbiol. Immunol.* **146**, 13–25
Brown, W. R., Newcomb, R. W., and Ishizake, K. (1970) *J. Clin. Invest.* **49**, 1374–1380
Drillian, R., and Spehner, D. (1983) *Virology* **131**, 385–393
Eiffert, H., Quentin, E., Decker, J., Hillemeir, S., Hufschmidt, M., Klingmüller, D., Weber, M. H., and Hilschman, N. (1984) *Hoppe-Seyler's Z. Physiol. Chem.* **365**, 1489–1495
Elsbein, A. D., Dorling, P. R., Vosbeck, K., and Horisberger, M. (1982) *J. Biol. Chem.* **257**, 1573–1576
Falk, P., Roth, K. A., Boren, T., Westblom, T. U., Gordon, J. I., and Normark, S. (1993) *Proc. Natl. Acad. Sci. U. S. A.* **90**, 2035–2039
Felgner, P. L., Gadek, T. R., Holm, M., Roman, R., Chan, H. W., Wenz, M., Northrop, J. P., Ringold, G. M., and Danielsen, M. (1987) *Proc. Natl. Acad. Sci. U. S. A.* **84**, 7413–7417
Frutiger, S., Hughes, G. J., Hanly, W. C., Kingzette, M., and Jaton, J.-C. (1986) *J. Biol. Chem.* **261**, 16673–16681
Garcia-Pardo, A., Lamm, M. E., Plaut, A. G., and Frangione, R. (1979) *Mol. Immunol.* **16**, 477–482
Hänggi, M., Bannwarth, W., and Stunnenberg, H. G. (1986) *EMBO J.* **5**, 1071–1076
Harlow, E., and Lane, D. (1988) *Antibodies: A Laboratory Manual*, Cold Spring Harbor Press, Cold Spring Harbor, NY
Higuchi, R. (1990) in *PCR Protocols: A Guide to Methods and Applications* (Innis, M. A., Gelfand, D. H., Sninsky, J. J., and White, T. J., eds) p. 177, Academic Press Inc., New York
Hirt, R., Hughes, G. J., Frutiger, S., Michetti, P., Perregaux, C., Poulain-Godefroy, O., Jeanguenat, N., Neutra, M. R., and Kraehenbuhl, J.-P. (1993) *Cell* **74**, 245–255
Hochuli, E., Döbeli, H., and Schacher, A. (1987) *J. Chromatogr.* **411**, 177–184
Jankneckt, R., De Martynoff, G., Lou, J., Hipkind, R. A., Nordheim, A., and Stunnenberg, H. G. (1991) *Proc. Natl. Acad. Sci. U. S. A.* **88**, 8972–8976
Kerr, M. A. (1990) *Biochem. J.* **271**, 285–296
Kozak, M. (1986) *Cell* **44**, 283–292
Kraehenbuhl, J.-P., and Neutra, M. R. (1992a) *Physiol. Rev.* **72**, 853–879
Kraehenbuhl, J.-P., and Neutra, M. R. (1992b) *Trends Cell Biol.* **2**, 134–138
Krajci, P., Solberg, R., Sandberg, M., Øyen, O., Jahnsen, T., and Brandtzaeg, P. (1989) *Biochem. Biophys. Res. Commun.* **158**, 783–789
Kühn, L. C., and Kraehenbuhl, J.-P. (1982) *Trends Biochem. Sci.* **7**, 299–302
Lee, C. R., Weltzin, R., Soman, G., Georgakopoulos, K. M., Houle, D. M., and Monath, T. P. (1994) *Infect. Immun.* **62**, 887–891
Lindh, E. (1975) *J. Immunol.* **114**, 284–286
Lindh, E., and Björk, I. (1977) *Acta Path. Microbiol. Scand.* **85**, 449–453
Mackett, J. M., Smith, S. M., and Moss, B. (1982) *Proc. Natl. Acad. Sci. U. S. A.* **79**, 7415–7419
Mackett, J. M., Smith, S. M., and Moss, B. (1984) *J. Virol.* **49**, 857–864
Malitschek, B., and Schartl, M. (1991) *BioTechniques* **11**, 177–178
McCune, J. M., Fu, S. M., and Kunkel, H. G. (1981) *J. Exp. Med.* **154**, 138–145
Mestecky, J., and McGhee, J. R. (1987) *Adv. Immunol.* **40**, 153–245
Mestecky, J., Lue, C., and Russell, M. W. (1991) *Gastroenterol. Clin. North Am.* **20**, 441–471
Miller, L. K. (1993) *Curr. Opin. Genet. Dev.* **3**, 97–101
Mizoguchi, A., Mizuochi, T., and Kobata, A. (1982) *J. Biol. Chem.* **257**, 9612–9621
Mestov, K. E., Friedländer, M., and Blobel, G. (1984) *Nature* **308**, 37–43
Neutra, M. R., and Kraehenbuhl, J.-P. (1994) *Am. J. Trop. Med. Hyg.* **50**, 10–13
Panicali, D., and Paoletti, E. (1982) *Proc. Natl. Acad. Sci. U. S. A.* **79**, 4927–4931
Parkhouse, R. M. E., and Della Corte, E. (1973) *Biochem. J.* **136**, 607–609
Parvin, J., Timmers, H., and Sharp, P. (1992) *Cell* **68**, 1135–1144
Piwnica-Worms, H. (1990) in *Current Protocols in Molecular Biology* (Ausubel. F. M., Brent, R., Kingston, R. E., Moore, D. D., Seidman, J. G., Smith, J. A., and Struhl, K., eds) Suppl. 13, John Wiley and Sons, New York
Porath, J., Carlsson, J., Olsson, I., and Belfrage, G. (1975) *Nature* **258**, 598–599
Putlitz, J. Z. (1990) *Bio/Technology* **8**, 651–654
Sambrook, J., Fritsch, E. F., and Maniatis, T. (1989) in *Molecular Cloning* (Nolan, C., ed) Second Edition, Cold Spring Harbor Laboratory Press, New York
Sanger, F., Nicklen, S., and Coulson, A. R. (1977) *Proc. Natl. Acad. Sci. U. S. A.* **74**, 5463–5467
Schaerer, E., Nautra, M. R., and Kraehenbuhl, J.-P. (1991) *J. Membr. Biol.* **123**, 93–103
Summers, M. D., and Smith, G. E. (1988) *Tex. Agric. Exp. Stn. Bull.* **1555**, 1–56
Tarentino, A. L., and Plummer, T. H. (1994) *Methods Enzymol.* **230**, 44–57
Taussig, R., Quarmby, L. M., and Gilman, A. G. (1993) *J. Biol. Chem.* **268**, 9–12
Underdown, B. J., and Derrington, K. J. (1974) *J. Immunol.* **112**, 949–959
Weltzin, R., Lucia-Jandris, P., Michetti, P., Fields, B. N., Kraehenbuhl, J.-P., and Neutra, M. R. (1989) *J. Cell Biol.* **108**, 1673–1685
Wessel, D., and Flügga, U. I. (1984) *Anal. Biochem.* **138**, 141–143